Chapter 1
Introduction and Historical Review

The subject of this book can be broadly described as the principles of radio interferometry applied to the measurement of natural radio signals from cosmic sources. The uses of such measurements lie mainly within the domains of astrophysics, astrometry, and geodesy. As an introduction, we consider in this chapter the applications of the technique, some basic terms and concepts, and the historical development of the instruments and their uses.

The fundamental concept of this book is that the image, or intensity distribution, of a source has a Fourier transform that is the two-point correlation function of the electric field, whose components can be directly measured by an interferometer. This Fourier transform is normally called the fringe visibility function, which in general is a complex quantity. The basic formulation of this principle is called the van Cittert–Zernike theorem (see Chap. 15), derived in the 1930s in the context of optics but not widely appreciated by radio astronomers until the publication of the well-known textbook *Principles of Optics* by Born and Wolf (1959). The techniques of radio interferometry developed from those of the Michelson stellar interferometer without specific knowledge of the van Cittert–Zernike theorem. Many of the principles of interferometry have counterparts in the field of X-ray crystallography (see Beevers and Lipson 1985).

1.1 Applications of Radio Interferometry

Radio interferometers and synthesis arrays, which are basically ensembles of two-element interferometers, are used to make measurements of the fine angular detail in the radio emission from the sky. The angular resolution of a single radio antenna is insufficient for many astronomical purposes. Practical considerations limit the resolution to a few tens of arcseconds. For example, the beamwidth of

A.R. Thompson, J.M. Moran, and G.W. Swenson Jr., *Interferometry and Synthesis in Radio Astronomy*, Astronomy and Astrophysics Library,
DOI 10.1007/978-3-319-44431-4_1

a 100-m-diameter antenna at 7-mm wavelength is approximately $17''$. In the optical range, the diffraction limit of large telescopes (diameter $\sim$ 8 m) is about $0.015''$, but the angular resolution achievable from the ground by conventional techniques (i.e., without adaptive optics) is limited to about $0.5''$ by turbulence in the troposphere. For progress in astronomy, it is particularly important to measure the positions of radio sources with sufficient accuracy to allow identification with objects detected in the optical and other parts of the electromagnetic spectrum [see, for example, Kellermann (2013)]. It is also very important to be able to measure parameters such as intensity, polarization, and frequency spectrum with similar angular resolution in both the radio and optical domains. Radio interferometry enables such studies to be made.

Precise measurement of the angular positions of stars and other cosmic objects is the concern of astrometry. This includes the study of the small changes in celestial positions attributable to the parallax introduced by the Earth's orbital motion, as well as those resulting from the intrinsic motions of the objects. Such measurements are an essential step in the establishment of the distance scale of the Universe. Astrometric measurements have also provided a means to test the general theory of relativity and to establish the dynamical parameters of the solar system. In making astrometric measurements, it is essential to establish a reference frame for celestial positions. A frame based on extremely distant high-mass objects as position references is close to ideal. Radio measurements of distant, compact, extragalactic sources presently offer the best prospects for the establishment of such a system. Radio techniques provide an accuracy of the order of 100 μas or less for absolute positions and 10 μas or less for the relative positions of objects closely spaced in angle. Optical measurements of stellar images, as seen through the Earth's atmosphere, allow the positions to be determined with a precision of about 50 mas. However, positions of 10^5 stars have been measured to an accuracy of $\sim$1 mas with the Hipparcos satellite (Perryman et al. 1997). The Gaia[1] mission is expected to provide the positions of 10^9 stars to an accuracy of $\sim$10 μas (de Bruijne et al. 2014).

As part of the measurement process, astrometric observations include a determination of the orientation of the instrument relative to the celestial reference frame. Ground-based observations therefore provide a measure of the variation of the orientation parameters for the Earth. In addition to the well-known precession and nutation of the direction of the axis of rotation, there are irregular shifts of the Earth's axis relative to the surface. These shifts, referred to as polar motion, are attributed to the gravitational effects of the Sun and Moon on the equatorial bulge of the Earth and to dynamic effects in the Earth's mantle, crust, oceans, and atmosphere. The same causes give rise to changes in the angular rotation velocity of the Earth, which are manifest as corrections that must be applied to the system of universal time. Measurements of the orientation parameters are important in the study of the dynamics of the Earth. During the 1970s, it became clear that radio techniques could provide an accurate measure of these effects, and in the late 1970s,

[1] An astrometric space observatory of the European Space Agency.

the first radio programs devoted to the monitoring of universal time and polar motion were set up jointly by the U.S. Naval Observatory and the U.S. Naval Research Laboratory, and also by NASA and the National Geodetic Survey. Polar motion can also be studied with satellites, in particular the Global Positioning System, but distant radio sources provide the best standard for measurement of Earth rotation.

In addition to revealing angular changes in the motion and orientation of the Earth, precise interferometer measurements entail an astronomical determination of the vector spacing between the antennas, which for spacings of $\sim$ 100 km or more is usually more precise than can be obtained by conventional surveying techniques. Very-long-baseline interferometry (VLBI) involves antenna spacings of hundreds or thousands of kilometers, and the uncertainty with which these spacings can be determined has decreased from a few meters in 1967, when VLBI measurements were first made, to a few millimeters. Relative motions of widely spaced sites on separate tectonic plates lie in the range 1–10 cm per year and have been tracked extensively with VLBI networks. Interferometric techniques have also been applied to the tracking of vehicles on the lunar surface and the determination of the positions of spacecraft. In this book, however, we limit our concern mainly to measurements of natural signals from astronomical objects.

The attainment of the highest angular resolution in the radio domain of the electromagnetic spectrum results in part from the ease with which radio frequency (RF) signals can be processed electronically with high precision. The use of the heterodyne principle to convert received RF signals to a convenient baseband, by mixing them with a signal from a local oscillator, is essential to this technology. A block diagram of an idealized standard receiving system (also known as a radiometer) is shown in Appendix 1.1. Another advantage in the radio domain is that the phase variations induced by the Earth's neutral atmosphere are less severe than at shorter wavelengths. Future technology will provide even higher resolution at infrared and optical wavelengths from observatories above the Earth's atmosphere. However, radio waves will remain of vital importance in astronomy since they reveal objects that do not radiate in other parts of the spectrum, and they are able to pass through galactic dust clouds that obscure the view in the optical range.

1.2 Basic Terms and Definitions

This section is written for readers who are unfamiliar with the basics of radio astronomy. It presents a brief review of some background information that is useful when approaching the subject of radio interferometry.

1.2.1 Cosmic Signals

The voltages induced in antennas by radiation from cosmic radio sources are generally referred to as *signals*, although they do not contain information in the usual engineering sense. Such signals are generated by natural processes and almost universally have the form of Gaussian random noise. That is to say, the voltage as a function of time at the terminals of a receiving antenna can be described as a series of very short pulses of random occurrence that combine as a waveform with Gaussian amplitude distribution. In a bandwidth $\Delta\nu$, the envelope of the radio frequency waveform has the appearance of random variations with timescale of order $1/\Delta\nu$. For most radio sources (except, for example, pulsars), the characteristics of the signals are invariant with time, at least on the scale of minutes or hours, the duration of a typical radio astronomy observation. Gaussian noise of this type is assumed to be identical in character to the noise voltages generated in resistors and amplifiers and is sometimes called Johnson noise. Such waveforms are usually assumed to be stationary and ergodic, that is, ensemble averages and time averages converge to equal values.

Most of the power is in the form of *continuum radiation*, the power spectrum of which shows gradual variation with frequency. For some wideband instruments, there may be significant variation within the receiver bandwidth. Figure 1.1 shows continuum spectra of eight different types of radio sources. Radio emission from the radio galaxy Cygnus A, the supernova remnant Cassiopeia A, and the quasar 3C48 is generated by the synchrotron mechanism [see, e.g., Rybicki and Lightman (1979), Longair (1992)], in which high-energy electrons in magnetic fields radiate as a result of their orbital motion. The radiating electrons are generally highly relativistic, and under these conditions, the radiation emitted by each one is concentrated in the direction of its instantaneous motion. An observer therefore sees pulses of radiation from those electrons whose orbital motion lies in, or close to, a plane containing the observer. The observed polarization of the radiation is mainly linear, and any circularly polarized component is generally quite small. The overall linear polarization from a source, however, is seldom large, since it is randomized by the variation of the direction of the magnetic field within the source and by Faraday rotation. The power in the electromagnetic pulses from the electrons is concentrated at harmonics of the orbital frequency, and a continuous distribution of electron energies results in a continuum radio spectrum. The individual pulses from the electrons are too numerous to be separable, and the electric field appears as a continuous Gaussian random process with zero mean. The variation of the spectrum as a function of frequency is related to the energy distribution of the electrons. At low frequencies, these spectra turn over due to the effect of self-absorption. M82 is an example of a starburst galaxy. At low frequencies, synchrotron emission dominates, but at high frequencies, emission from dust grains at a temperature of about 45K and emissivity of 1.5 dominates. TW Hydrae is a star with a protoplanetary disk whose emission at radio frequencies is dominated by dust at a temperature of about 30K and emissivity of 0.5.

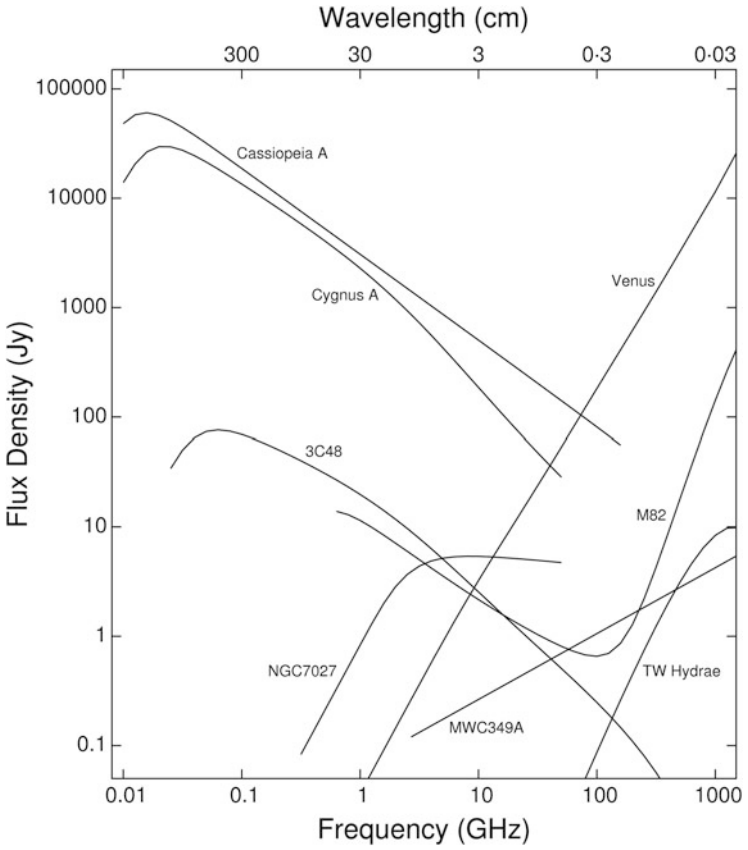

Fig. 1.1 Examples of spectra of eight different types of discrete continuum sources: Cassiopeia A [supernova remnant, Baars et al. (1977)], Cygnus A [radio galaxy, Baars et al. (1977)], 3C48 [quasar, Kellermann and Pauliny-Toth (1969)], M82 [starburst galaxy, Condon (1992)], TW Hydrae [protoplanetary disk, Menu et al. (2014)], NGC7207 [planetary nebula, Thompson (1974)], MWC349A [ionized stellar wind, Harvey et al. (1979)], and Venus [planet, at 9.6″ diameter (opposition), Gurwell et al. (1995)]. For practical purposes, we define the edges of the radio portion of the electromagnetic spectrum to be set by the limits imposed by ionospheric reflection at low frequencies ($\sim$ 10 MHz) and to atmospheric absorption at high frequencies ($\sim$ 1000 GHz). Some of the data for this table were taken from NASA/IPAC Extragalactic Database (2013) [One jansky (Jy) = 10^{-26} W m^{-2} Hz^{-1}].

NGC7027, the spectrum of which is shown in Fig. 1.1, is a planetary nebula within our Galaxy in which the gas is ionized by radiation from a central star. The radio emission is a thermal process and results from free-free collisions between unbound electrons and ions within the plasma. At the low-frequency end of the spectral curve, the nebula is opaque to its own radiation and emits a blackbody spectrum. As the frequency increases, the absorptivity, and hence the emissivity, decrease approximately as ν^{-2} [see, e.g., Rybicki and Lightman (1979)], where ν is the frequency. This behavior counteracts the ν^2 dependence of the Rayleigh–Jeans

law, and thus the spectrum becomes nearly flat when the nebula is no longer opaque to the radiation. Radiation of this type is randomly polarized. MWC349A is an example of an inhomogeneous ionized gas expanding at constant velocity in a stellar envelope, which gives rise to a spectral dependence of $\nu^{0.6}$.

At millimeter wavelengths, opaque thermal sources such as planetary bodies become very strong and often serve as calibrators. Venus has a brightness temperature that varies from 700K (the surface temperature) at low frequencies to 250K (the atmospheric temperature) at high frequencies.

In contrast with continuum radiation, *spectral line radiation* is generated at specific frequencies by atomic and molecular processes. A fundamentally important line is that of neutral atomic hydrogen at 1420.405 MHz, which results from the transition between two energy levels of the atom, the separation of which is related to the spin vector of the electron in the magnetic field of the nucleus. The natural width of the hydrogen line is negligibly small ($\sim 10^{-15}$ Hz), but Doppler shifts caused by thermal motion of the atoms and large-scale motion of gas clouds spread the line radiation. The overall Doppler spread within our Galaxy covers several hundred kilohertz. Information on galactic structure is obtained by comparison of these velocities with those of models incorporating galactic rotation.

Our Galaxy and others like it also contain large molecular clouds at temperatures of 10–100 K in which new stars are continually forming. These clouds give rise to many atomic and molecular transitions in the radio and far-infrared ranges. More than 4,500 molecular lines from approximately 180 molecular species have been observed [see Herbst and van Dishoeck (2009)]. Lists of atomic and molecular lines are given by Jet Propulsion Laboratory (2016), the University of Cologne (2016), and Splatalogue (2016). For earlier lists, see Lovas et al. (1979) and Lovas (1992). A few of the more important lines are given in Table 1.1. Note that this table contains less than 1% of the known lines in the frequency range below 1 THz. Figure 1.2 shows the spectrum of radiation of many molecular lines from the Orion Nebula in the bands from 214 to 246 and from 328 to 360 GHz. Although the radio window in the Earth's atmosphere ends above $\sim$ 1 THz, sensitive submillimeter- and millimeter-wavelength arrays can detect such lines as the $^2P_{3/2} \rightarrow {}^2P_{1/2}$ line of CII at 1.90054 THz (158 μm), which are Doppler shifted into the radio window for redshifts (z) greater than $\sim$ 2. Some of the lines, notably those of OH, H_2O, SiO, and CH_3OH, show very intense emission from sources of very small apparent angular diameter. This emission is generated by a maser process [see, e.g., Reid and Moran (1988), Elitzur (1992), and Gray (2012)].

The strength of the radio signal received from a discrete source is expressed as the *spectral flux density*, or *spectral power flux density*, and is measured in watts per square meter per hertz (W m^{-2} Hz^{-1}). For brevity, astronomers often refer to this quantity as *flux density*. The unit of flux density is the jansky (Jy); 1 Jy = 10^{-26} W m^{-2} Hz^{-1}. It is used for both spectral line and continuum radiation. The measure of radiation integrated in frequency over a spectral band has units of W m^{-2} and is referred to as *power flux density*. In the standard definition of the IEEE (1977), power flux density is equal to the time average of the Poynting vector of the wave. In producing an image of a radio source, the desired quantity is the power flux density

Table 1.1 Some important radio lines

Chemical name	Chemical formula	Transition	Frequency (GHz)
Deuterium	D	$^2S_{1/2},\ F = \frac{3}{2} \rightarrow \frac{1}{2}$	0.327
Hydrogen	H	$^2S_{1/2},\ F = 1 \rightarrow 0$	1.420
Hydroxyl radical	OH	$^2\Pi_{3/2},\ J = 3/2,\ F = 1 \rightarrow 2$	1.612[a]
Hydroxyl radical	OH	$^2\Pi_{3/2},\ J = 3/2,\ F = 1 \rightarrow 1$	1.665[a]
Hydroxyl radical	OH	$^2\Pi_{3/2},\ J = 3/2,\ F = 2 \rightarrow 2$	1.667[a]
Hydroxyl radical	OH	$^2\Pi_{3/2},\ J = 3/2,\ F = 2 \rightarrow 1$	1.721[a]
Methyladyne	CH	$^2\Pi_{1/2},\ J = 1/2,\ F = 1 \rightarrow 1$	3.335
Hydroxyl radical	OH	$^2\Pi_{1/2},\ J = 1/2,\ F = 1 \rightarrow 0$	4.766[a]
Formaldehyde	H_2CO	$1_{10} - 1_{11}$, six F transitions	4.830
Hydroxyl radical	OH	$^2\Pi_{3/2},\ J = 5/2,\ F = 3 \rightarrow 3$	6.035[a]
Methanol	CH_3OH	$5_1 \rightarrow 6_0\ A^+$	6.668[a]
Helium	$^3He^+$	$^2S_{1/2},\ F = 1 \rightarrow 0$	8.665
Methanol	CH_3OH	$2_0 \rightarrow 3_{-1}\ E$	12.179[a]
Formaldehyde	H_2CO	$2_{11} \rightarrow 2_{12}$, four F transitions	14.488
Cyclopropenylidene	C_3H_2	$1_{10} \rightarrow 1_{01}$	18.343
Water	H_2O	$6_{16} \rightarrow 5_{23}$, five F transitions	22.235[a]
Ammonia	NH_3	$1,\ 1 \rightarrow 1,\ 1$, eighteen F transitions	23.694
Ammonia	NH_3	$2,\ 2 \rightarrow 2,\ 2$, seven F transitions	23.723
Ammonia	NH_3	$3,\ 3 \rightarrow 3,\ 3$, seven F transitions	23.870
Methanol	CH_3OH	$6_2 \rightarrow 6_1,\ E$	25.018
Silicon monoxide	SiO	$v = 2,\ J = 1 \rightarrow 0$	42.821[a]
Silicon monoxide	SiO	$v = 1,\ J = 1 \rightarrow 0$	43.122[a]
Carbon monosulfide	CS	$J = 1 \rightarrow 0$	48.991
Silicon monoxide	SiO	$v = 1,\ J = 2 \rightarrow 1$	86.243[a]
Hydrogen cyanide	HCN	$J = 1 \rightarrow 0$, three F transitions	88.632
Formylium	HCO^+	$J = 1 \rightarrow 0$	89.189
Diazenylium	N_2H^+	$J = 1 \rightarrow 0$, seven F transitions	93.174
Carbon monosulfide	CS	$J = 2 \rightarrow 1$	97.981
Carbon monoxide	$^{12}C^{18}O$	$J = 1 \rightarrow 0$	109.782
Carbon monoxide	$^{13}C^{16}O$	$J = 1 \rightarrow 0$	110.201
Carbon monoxide	$^{12}C^{17}O$	$J = 1 \rightarrow 0$, three F transitions	112.359
Carbon monoxide	$^{12}C^{16}O$	$J = 1 \rightarrow 0$	115.271
Carbon monosulfide	CS	$J = 3 \rightarrow 2$	146.969
Water	H_2O	$3_{13} \rightarrow 2_{20}$	183.310[a]
Carbon monoxide	$^{12}C^{16}O$	$J = 2 \rightarrow 1$	230.538
Carbon monosulfide	CS	$J = 5 \rightarrow 4$	244.936
Water	H_2O	$5_{15} \rightarrow 4_{22}$	325.153[a]
Carbon monosulfide	CS	$J = 7 \rightarrow 6$	342.883
Carbon monoxide	$^{12}C^{16}O$	$J = 3 \rightarrow 2$	345.796
Water	H_2O	$4_{14} \rightarrow 3_{21}$	380.197[b]
Carbon monoxide	$^{12}C^{16}O$	$J = 4 \rightarrow 3$	461.041
Heavy water	HDO	$1_{01} \rightarrow 0_{00}$	464.925
Carbon	C	$^3P_1 \rightarrow {}^3P_0$	492.162
Water	H_2O	$1_{10} \rightarrow 1_{01}$	556.936[b]
Ammonia	NH_3	$1_0 \rightarrow 0_0$	572.498
Carbon monoxide	$^{12}C^{16}O$	$J = 6 \rightarrow 5$	691.473
Carbon monoxide	$^{12}C^{16}O$	$J = 7 \rightarrow 6$	806.652
Carbon	C	$^3P_2 \rightarrow {}^3P_1$	809.340

[a]Strong maser transition.
[b]High atmospheric opacity (see Fig. 13.14).

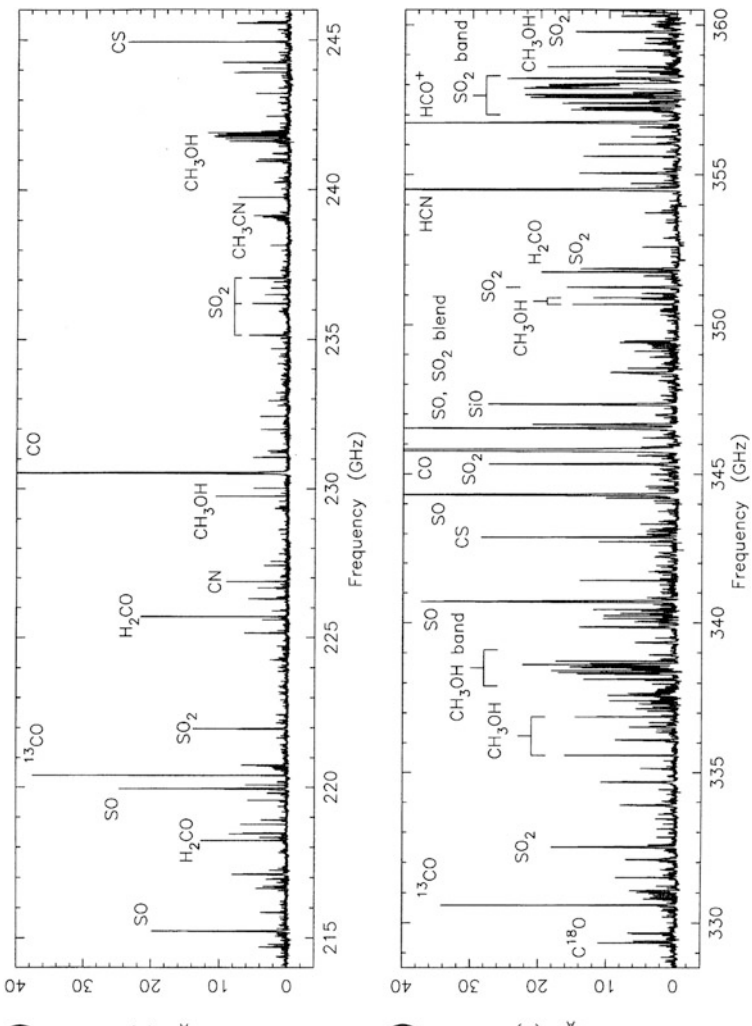

Fig. 1.2 Spectrum of the Orion Nebula for 214–246 and 328–360 GHz. The ordinate is antenna temperature corrected for atmospheric absorption, which is proportional to the power received. The frequency scale has been corrected for motion of the Earth with respect to the local standard of rest. The spectral resolution is 1 MHz, which corresponds to a velocity resolution of 1.3 and 0.87 km s^{-1} at 230 and 345 GHz, respectively. Note the higher density of lines in the higher frequency band. The measurements shown in (**a**) are from Blake et al. (1987), and those in (**b**) are from Schilke et al. (1997).

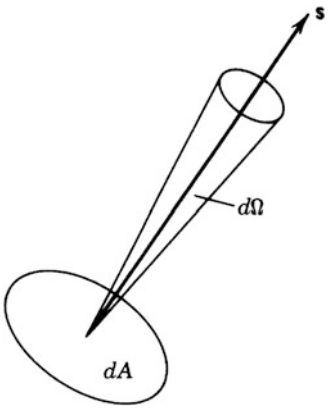

Fig. 1.3 Elements of solid angle and surface area illustrating the definition of intensity. *dA* is normal to **s**.

emitted per unit solid angle subtended by the radiating surface, which is measured in units of W m^{-2} Hz^{-1} sr^{-1}. This quantity is variously referred to as the *intensity, specific intensity*, or *brightness* of the radiation. In radio astronomical imaging, we can measure the intensity in only two dimensions on the surface of the celestial sphere, and the measured emission is the component normal to that surface, as seen by the observer.

In radiation theory, the quantity intensity, or specific intensity, often represented by I_ν, is the measure of radiated energy flow per unit area, per unit time, per unit frequency bandwidth, and per unit solid angle. Thus, in Fig. 1.3, the power flowing in direction **s** within solid angle $d\Omega$, frequency band $d\nu$, and area dA is $I_\nu(\mathbf{s})\, d\Omega\, d\nu\, dA$. This can be applied to emission from the surface of a radiating object, to propagation through a surface in space, or to reception on the surface of a transducer or detector. The last case applies to reception in an antenna, and the solid angle then denotes the area of the celestial sphere from which the radiation emanates. Note that in optical astronomy, the specific intensity is usually defined as the intensity per unit bandwidth I_λ, where $I_\lambda = I_\nu \nu^2/c$, and c is the speed of light [see, e.g., Rybicki and Lightman (1979)].

For thermal radiation from a blackbody, the intensity is related to the physical temperature T of the radiating matter by the Planck formula, for which

$$I_\nu = \frac{2kT\nu^2}{c^2}\left[\frac{\frac{h\nu}{kT}}{e^{h\nu/kT}-1}\right], \tag{1.1}$$

where k is Boltzmann's constant, and h is Planck's constant. When $h\nu \ll kT$, we can use the Rayleigh–Jeans approximation, in which case the expression in the square brackets is replaced by unity. The Rayleigh–Jeans approximation requires ν (GHz) $\ll 20\ T$ (K) and is violated at high frequencies and low temperatures in many situations of interest to radio astronomers. However, for any radiation

mechanism, a brightness temperature T_B can be defined:

$$T_B = \frac{c^2 I_\nu}{2k\nu^2} \,. \tag{1.2}$$

In the Rayleigh–Jeans domain, the brightness temperature T_B is that of a blackbody at physical temperature $T = T_B$. In the examples in Fig. 1.1, T_B is of the order of 10^4 K for NGC7027 and corresponds to the electron temperature. For Cygnus A and 3C48, T_B is of the order of 10^8 K or greater and is a measure of the energy density of the electrons and the magnetic fields, not a physical temperature. As a spectral line example, T_B for the carbon monoxide (CO) lines from molecular clouds is typically 10–100 K. In this case, T_B is proportional to the excitation temperature associated with the energy levels of the transition and is related to the temperature and density of the gas as well as to the temperature of the radiation field.

1.2.2 Source Positions and Nomenclature

The positions of radio sources are measured in the celestial coordinates *right ascension* and *declination*. On the celestial sphere, these quantities are analogous, respectively, to longitude and latitude on the Earth but tied to the plane of the Earth's orbit around the Sun. The zero of right ascension is arbitrarily chosen as the point at which the Sun crosses the celestial equator (going from negative to positive declination) on the vernal equinox at the first point of Aries at a given epoch. Positions of objects in celestial coordinates vary as a result of precession and nutation of the Earth's axis of rotation, aberration, and proper motion. These positions are usually listed for the standard epoch of the year 2000. Former standard epochs were 1950 and 1900. Methods of naming sources have proceeded haphazardly over the centuries. Important optical catalogs of sources were constructed as numerical lists, often in order of right ascension. Examples include the Messier catalog of nonstellar objects (Messier 1781; now containing 110 objects identified as galaxies, nebulae, and star clusters), the New General Catalog of nonstellar sources (Dreyer 1888; originally with 7,840 objects, mostly galaxies), and the Henry Draper catalog of stars (Cannon and Pickering 1924; now with 359,083 entries). The earliest radio sources were designated by their associated constellation. Hence, Cygnus A is the strongest source in the constellation of Cygnus. As the radio sky was systematically surveyed, catalogs appeared such as the third Cambridge catalog (3C), with 471 entries in the original list [Edge et al. (1959), extragalactic sources, e.g., 3C273] and the Westerhout catalog of 81 sources along the galactic plane [Westerhout (1958); mostly ionized nebula, e.g., W3].

In 1974, the International Astronomical Union adopted a resolution (International Astronomical Union 1974) to standardize the naming of sources based on their coordinates in the epoch of 1950 called the 4 + 4 system, in which the first four characters give the hour and minutes of right ascension (RA); the fifth, the

sign of the declination (Dec.); and the remaining three, the degrees and tenths of degrees of declination. For example, the source at RA $01^{\mathrm{h}}34^{\mathrm{m}}49.83^{\mathrm{s}}$, Dec. $32°54'20.5''$ would be designated 0134+329. Note that coordinates were truncated, not rounded. This system no longer has the accuracy needed to distinguish among sources. The current recommendation of the IAU Task Group on Astronomical Designations [International Astronomical Union (2008); see also NASA/IPAC Extragalactic Database (2013)] recommends the following convention. The source name begins with an identification acronym followed by a letter to identify the type of coordinates, followed by the coordinates to requisite accuracy. Examples of identification acronyms are QSO (quasi-stellar object), PSR (pulsar), and PKS (Parkes Radio Source). Coordinate identifiers are usually limited to J for epoch 2000, B for epoch 1950, and G for galactic coordinates. Hence, the radio source at the center of the galaxy M87, also known as NGC4486, contains an active galactic nucleus (AGN) centered at RA $= 12^{\mathrm{h}}30^{\mathrm{m}}49.42338^{\mathrm{s}}$, Dec. $= 12°23'28.0439''$, which might be designated AGN J1230494233+122328043. It is also well known by the designations Virgo A and 3C274. Many catalogs of radio sources have been made, and some of them are described in Sect. 1.3.8. An index of more than 50 catalogs made before 1970, identifying more than 30,000 extragalactic radio sources, was compiled by Kesteven and Bridle (1971).

An example of a more recent survey is the NRAO VLA Sky Survey (NVSS) conducted by Condon et al. (1998) using the Very Large Array (VLA) at 1.4 GHz, which contains approximately 2×10^6 sources (about one source per 100 beam solid angles). Another important catalog derived from VLBI observations is the International Celestial Reference Frame (ICRF), which contains 295 sources with positions accurate to about 40 microarcseconds (Ma et al. 1998; Fey et al. 2015).

1.2.3 Reception of Cosmic Signals

The antennas used most commonly in radio astronomy are of the reflector type mounted to allow tracking over most of the sky. The exceptions are mainly instruments designed for meter or longer wavelengths. The collecting area A of a reflector antenna, for radiation incident in the center of the main beam, is equal to the geometrical area multiplied by an aperture efficiency factor, which is typically within the range 0.3–0.8. The received power P_A delivered by the antenna to a matched load in a bandwidth $\Delta\nu$, from a randomly polarized source of flux density S, assumed to be small compared to the beamwidth, is given by

$$P_A = \tfrac{1}{2} SA\Delta\nu \ . \tag{1.3}$$

Note that S is the intensity I_ν integrated over the solid angle of the source. The factor $\frac{1}{2}$ takes account of the fact that the antenna responds to only one-half the power in the randomly polarized wave. It is often convenient to express random noise power, P, in terms of an effective temperature T, as

$$P = kT\Delta\nu \ , \tag{1.4}$$

where k is Boltzmann's constant. In the Rayleigh–Jeans domain, P is equal to the noise power delivered to a matched load by a resistor at physical temperature T (Nyquist 1928). In the general case, if we use the Planck formula [Eq. (1.1)], we can write $P = kT_{\text{Planck}}\Delta\nu$, where T_{Planck} is an effective radiation temperature, or noise temperature, of a load at physical temperature T, and is given by

$$T_{\text{Planck}} = T\left[\frac{\frac{h\nu}{kT}}{e^{h\nu/kT}-1}\right] . \tag{1.5}$$

The noise power in a receiving system (see Appendix 1.1) can be specified in terms of the *system temperature* T_S associated with a matched resistive load that would produce an equal power level in an equivalent noise-free receiver when connected to the input terminals. T_S is defined as the power available from this load divided by $k\Delta\nu$. In terms of the Planck formula, the relation between T_S and the physical temperature, T, of such a load is given by replacing T_{Planck} by T_S in Eq. (1.1).

The system temperature consists of two parts: T_R, the *receiver temperature*, which represents the internal noise from the receiver components, plus the unwanted noise incurred from connecting the receiver to the antenna and from the noise components from the antenna produced by ground radiation, atmospheric emission, ohmic losses, and other sources.

We reserve the term *antenna temperature* to refer to the component of the power received by the antenna that results from a cosmic source under study. The power received in an antenna from the source is [see Eq. (1.4)]

$$P_A = kT_A\,\Delta\nu\ , \tag{1.6}$$

and T_A is related to the flux density by Eqs. (1.3) and (1.6). It is useful to express this relation as $T_A\ (\text{K}) = SA/2k = S\ (\text{Jy}) \times A\ (\text{m}^2)/2800$. Astronomers sometimes specify the performance of an antenna in terms of *janskys per kelvin*, that is, the flux density (in units of 10^{-26} W m^{-2} Hz^{-1}), of a point source that increases T_A by one kelvin. Thus, this measure is equal to $2800/A\ (\text{m}^2)$ Jy K^{-1}.

Another term that may be encountered is the *system equivalent flux density*, SEFD, which is an indicator of the combined sensitivity of both an antenna and receiving system. It is equal to the flux density of a point source in the main beam of the antenna that would cause the noise power in the receiver to be twice that of the system noise in the absence of a source. Equating P_A in Eq. (1.3) with $kT_S\Delta\nu$, we obtain

$$\text{SEFD} = \frac{2kT_S}{A} . \tag{1.7}$$

The ratio of the signal power from a source to the noise power in the receiving amplifier is T_A/T_S. Because of the random nature of the signal and noise, measurements of the power levels made at time intervals separated by $(2\Delta\nu)^{-1}$ can be considered independent. A measurement in which the signal level is averaged for

a time τ contains approximately $2\Delta\nu\tau$ independent samples. The signal-to-noise ratio (SNR), $\mathcal{R}_{\rm sn}$, at the output of a power-measuring device attached to the receiver is increased in proportion to the square root of the number of independent samples and is of the form

$$\mathcal{R}_{\rm sn} = C\frac{T_A}{T_S}\sqrt{\Delta\nu\tau}\ , \tag{1.8}$$

where C is a constant that is greater than or equal to one. This result (derived in Appendix 1.1) appears to have been first obtained by Dicke (1946) for an analog system. $C = 1$ for a simple power-law receiver with a rectangular passband and can be larger by a factor of ~ 2 for more complicated systems. Typical values of $\Delta\nu$ and τ are of order 1 GHz and 6 h, which result in a value of 4×10^6 for the factor $(\Delta\nu\tau)^{1/2}$. As a result, it is possible to detect a signal for which the power level is less than 10^{-6} times the system noise. A particularly effective use of long averaging time is found in the observations with the Cosmic Background Explorer (COBE) satellite, in which it was possible to measure structure at a brightness temperature level less than 10^{-7} of the system temperature (Smoot et al. 1990, 1992).

The following calculation may help to illustrate the low energies involved in radio astronomy. Consider a large radio telescope with a total collecting area of 10^4 m^2 pointed toward a radio source of flux density 1 mJy ($= 10^{-3}$ Jy) and accepting signals over a bandwidth of 50 MHz. In 10^3 years, the total energy accepted is about 10^{-7} J (1 erg), which is comparable to a few percent of the kinetic energy in a single falling snowflake. To detect the source with the same telescope and a system temperature of 50 K would require an observing time of about 5 min, during which time the energy received would be about 10^{-15} J.

1.3 Development of Radio Interferometry

1.3.1 Evolution of Synthesis Techniques

This section presents a brief history of interferometry in radio astronomy. As an introduction, the following list indicates some of the more important steps in the progress from the Michelson stellar interferometer to the development of multi-element, synthesis imaging arrays and VLBI:

1. *Michelson stellar interferometer.* This optical instrument introduced the technique of using two spaced receiving apertures, and the measurement of fringe amplitude to determine angular width (1890–1921).
2. *First astronomical observations with a two-element radio interferometer.* Ryle and Vonberg (1946), solar observations.
3. *Phase-switching interferometer.* First implementation of the voltage-multiplying action of a correlator, which is the device used to combine the signals from two antennas (1952).

4. *Astronomical calibration.* Gradual accumulation during the 1950s and 1960s of accurate positions for small-diameter radio sources from optical identifications and other means. Observations of such sources enabled accurate calibration of interferometer baselines and instrumental phases.
5. *Early measurements of angular dimensions of sources.* Use of variable-baseline interferometers ($\sim$ 1952 onward).
6. *Solar arrays.* Development of multiantenna arrays of centimeter-wavelength tracking antennas that provided detailed maps and profiles of the solar disk (mid-1950s onward).
7. *Arrays of tracking antennas.* General movement from meter-wavelength, non-tracking antennas to centimeter-wavelength, tracking antennas. Development of multielement arrays with a separate correlator for each baseline ($\sim$ 1960s).
8. *Earth-rotation synthesis.* Introduced by Ryle with some precedents from solar imaging. The development of computers to control receiving systems and perform Fourier transforms required in imaging was an essential component (1962).
9. *Spectral line capability.* Introduced into radio interferometry ($\sim$ 1962).
10. *Development of image-processing techniques.* Based on phase and amplitude closure, nonlinear deconvolution and other techniques, as described in Chaps. 10 and 11 ($\sim$ 1974 onward).
11. *Very-long-baseline interferometry* (*VLBI*). First observations (1967). Superluminal motion in active galactic nuclei discovered (1971). Contemporary plate motion detected (1986). International Celestial Reference Frame adopted (1998).
12. *Millimeter-wavelength instruments* ($\sim$ 100–300 GHz). Major developments mid-1980s onward.
13. *Orbiting VLBI (OVLBI).* U.S. Tracking and Data Relay Satellite System (TDRSS) experiment (1986–88). VLBI Space Observatory Programme (VSOP) (1997). RadioAstron (2011).
14. *Submillimeter-wavelength instruments* (300 GHz–1 THz). James Clerk Maxwell Telescope–Caltech Submillimeter Observatory interferometer (1992). Submillimeter Array of the Smithsonian Astrophysical Observatory (SAO) and Academia Sinica of Taiwan (2004). Atacama Large Millimeter/submillimeter Array (ALMA) (2013).

1.3.2 Michelson Interferometer

Interferometric techniques in astronomy date back to the optical work of Michelson (1890, 1920) and of Michelson and Pease (1921), who were able to obtain sufficiently fine angular resolution to measure the diameters of some of the nearer and larger stars such as Arcturus and Betelgeuse. The basic similarity of the theory of radio and optical radiation fields was recognized early by radio astronomers,

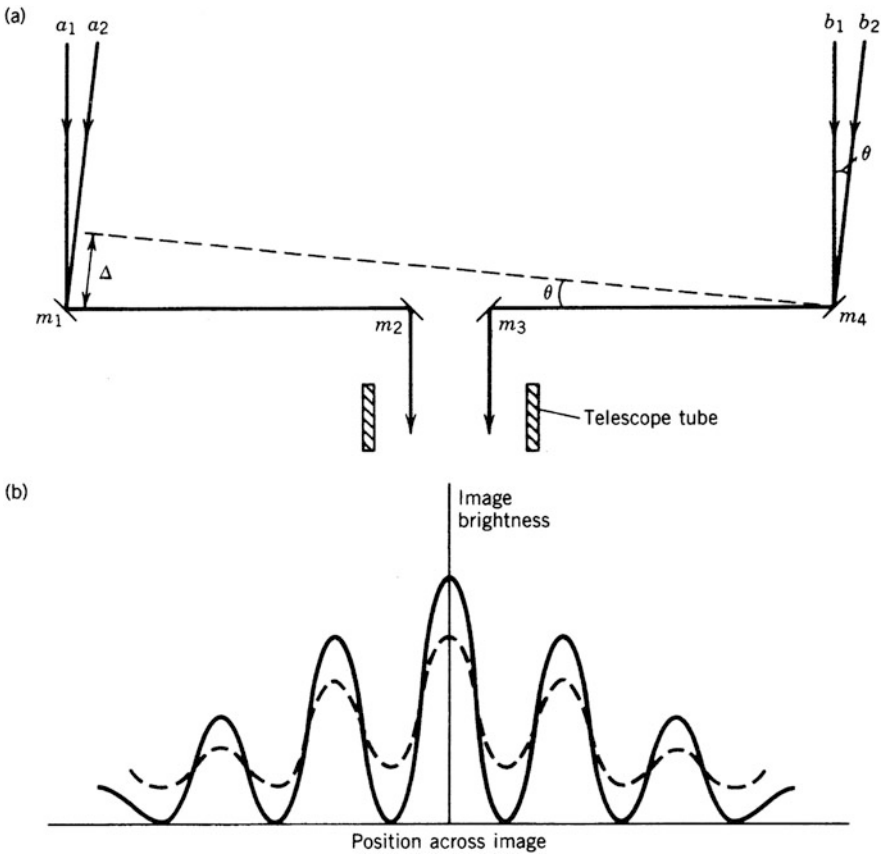

Fig. 1.4 (**a**) Schematic diagram of the Michelson–Pease stellar interferometer. The incoming rays are guided into the telescope aperture by mirrors m_1 to m_4, of which the outer pair define the two apertures of the interferometer. Rays a_1 and b_1 traverse equal paths to the eyepiece at which the image is formed, but rays a_2 and b_2, which approach at an angle θ to the instrumental axis, traverse paths that differ by a distance Δ. (**b**) The intensity of the image as a function of position angle in a direction parallel to the spacing of the interferometer apertures. The solid line shows the fringe profiles for an unresolved star ($\mathcal{V}_M = 1.0$), and the broken line is for a partially resolved star for which $\mathcal{V}_M = 0.5$.

and optical experience has provided valuable precedents to the theory of radio interferometry.

As shown in Fig. 1.4, beams of light from a star fall upon two apertures and are combined in a telescope. The resulting stellar image has a finite width and is shaped by effects that include atmospheric turbulence, diffraction at the mirrors, and the bandwidth of the radiation. Maxima in the light intensity resulting from interference occur at angles θ for which the difference Δ in the path lengths from the star to the point at which the light waves are combined is an integral number of wavelengths at the effective center of the optical passband. If the angular width of the star is

small compared with the spacing in θ between adjacent maxima, the image of the star is crossed by alternate dark and light bands, known as interference fringes. If, however, the width of the star is comparable to the spacing between maxima, one can visualize the resulting image as being formed by the superposition of images from a series of points across the star. The maxima and minima of the fringes from different points do not coincide, and the fringe amplitude is attenuated, as shown in Fig. 1.4b. As a measure of the relative amplitude of the fringes, Michelson defined the *fringe visibility*, $\mathcal{V}_M$, as

$$\mathcal{V}_M = \frac{\text{intensity of maxima - intensity of minima}}{\text{intensity of maxima + intensity of minima}} \,. \tag{1.9}$$

Note that with this definition, the visibility is normalized to unity when the intensity at the minima is zero, that is, when the width of the star is small compared with the fringe width. If the fringe visibility is measurably less than unity, the star is said to be *resolved* by the interferometer. In their 1921 paper, Michelson and Pease explained the apparent paradox that their instrument could be used to detect structure smaller than the seeing limit imposed by atmospheric turbulence. The fringe pattern, as depicted in Fig. 1.4, moves erratically on time scales of 10–100 ms. Over long averaging time, the fringes are smoothed out. However, the "jittering" fringes can be discerned by the human eye, which has a typical response time of tens of milliseconds.

Let $I(l, m)$ be the two-dimensional intensity of the star, or of a source in the case of a radio interferometer. (l, m) are coordinates on the sky, with l measured parallel to the aperture spacing vector and m normal to it. The fringes provide resolution in a direction parallel to the aperture spacing only. In the orthogonal direction, the response is simply proportional to the intensity integrated over solid angle. Thus, the interferometer measures the intensity projected onto the l direction, that is, the one-dimensional profile $I_1(l)$ given by

$$I_1(l) = \int I(l, m)\, dm \,. \tag{1.10}$$

As will be shown in later chapters, the fringe visibility is proportional to the modulus of the Fourier transform of $I_1(l)$ with respect to the spacing of the apertures measured in wavelengths. Figure 1.5 shows the integrated profile I_1 for three simple models of a star or radio source and the corresponding fringe visibility as a function of u, the spacing of the interferometer apertures in units of the wavelength. At the top of the figure is a rectangular pillbox distribution, in the center a circular pillbox, and at the bottom a circular Gaussian function. The rectangular pillbox represents a uniformly bright rectangle on the sky with sides parallel to the l and m axes and width a in the l direction. The circular pillbox represents a uniformly bright circular disk of diameter a. When projected onto the l axis, the one-dimensional intensity function I_1 has a semicircular profile. The Gaussian model is a circularly symmetric source with Gaussian taper of the intensity from the maximum at the center. The

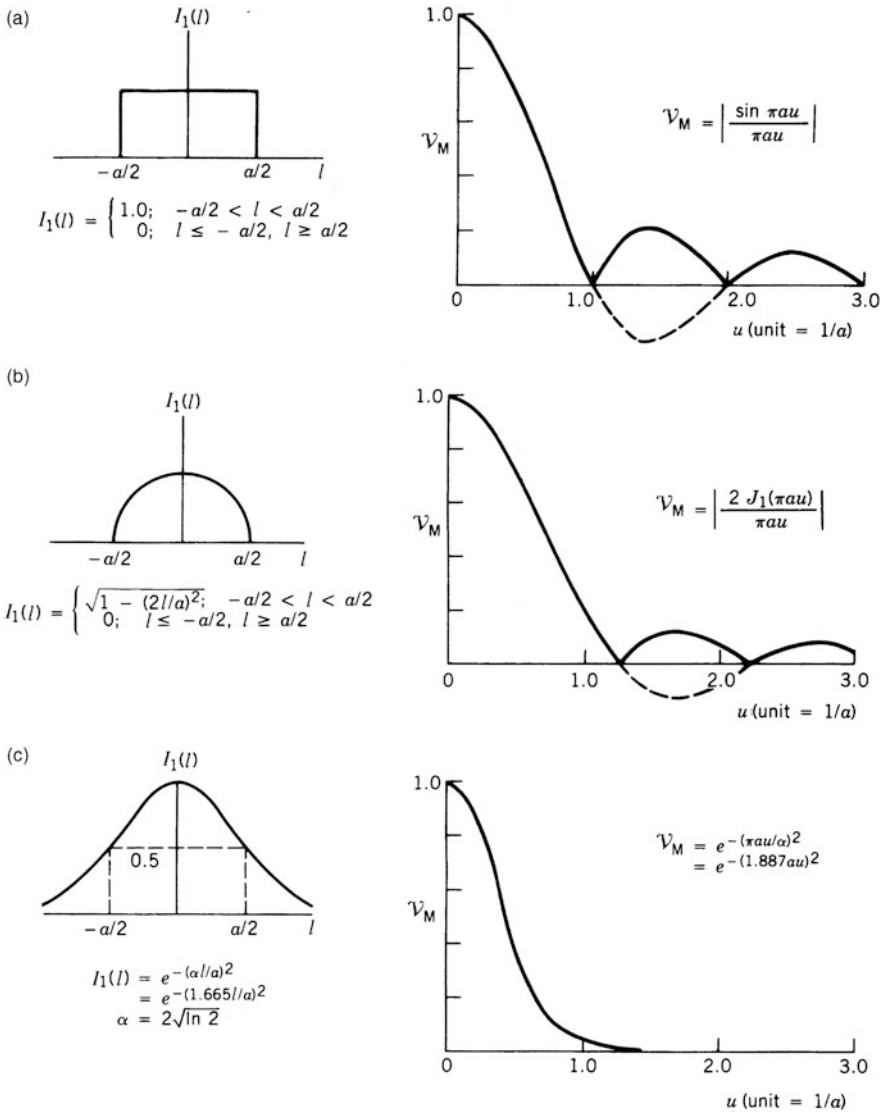

Fig. 1.5 The one-dimensional intensity profiles $I_1(l)$ for three simple intensity models: (**a**) left, a uniform rectangular source; (**b**) left, a uniform circular source; and (**c**) left, a circular Gaussian distribution. The corresponding Michelson visibility functions $\mathcal{V}_M$ are on the right. l is an angular variable on the sky, u is the spacing of the receiving apertures measured in wavelengths, and a is the characteristic angular width of the model. The solid lines in the curves of $\mathcal{V}_M$ indicate the modulus of the Fourier transform of $I_1(l)$, and the broken lines indicate negative values of the transform. See text for further explanation. Models are discussed in more detail in Sect. 10.4.

intensity is proportional to $\exp[-4\ln 2(l^2+m^2)/a^2]$, resulting in circular contours and a diameter a at the half-intensity level. Any slice through the model in a plane perpendicular to the (l,m) plane has a Gaussian profile with the same half-height width, a.

Michelson and Pease used mainly the circular disk model to interpret their observations and determined the stellar diameter by varying the aperture spacing of the interferometer to locate the first minimum in the visibility function. In the age before electronic instrumentation, the adjustment of such an instrument and the visual estimation of $\mathcal{V}_M$ required great care, since, as described above, the fringes were not stable but vibrated across the image in a random manner as a result of atmospheric fluctuations. The published results on stellar diameters measured with this method were never extended beyond the seven bright stars in Pease's (1931) list; for a detailed review see Hanbury Brown (1968). However, the use of electro-optical techniques now offers much greater instrumental capabilities in optical interferometry, as discussed in Sect. 17.4.

1.3.3 Early Two-Element Radio Interferometers

In 1946, Ryle and Vonberg constructed a radio interferometer to investigate cosmic radio emission, which had been discovered and verified by earlier investigators (Jansky 1933; Reber 1940; Appleton 1945; Southworth 1945). This interferometer used dipole antenna arrays at 175 MHz, with a baseline (i.e., the spacing between the antennas) that was variable between 10 and 140 wavelengths (17 and 240 m). A diagram of such an instrument and the type of record obtained are shown in Fig. 1.6. In this and most other meter-wavelength interferometers of the 1950s and 1960s, the antenna beams were pointed in the meridian, and the rotation of the Earth provided scanning in right ascension.

The receiver in Fig. 1.6 is sensitive to a narrow band of frequencies, and a simplified analysis of the response of the interferometer can be obtained in terms of monochromatic signals at the center frequency ν_0. We consider the signal from a radio source of very small angular diameter that is sufficiently distant that the incoming wavefront effectively lies in a plane. Let the signal voltage from the right antenna in Fig. 1.6 be represented by $V\sin(2\pi\nu_0 t)$. The longer path length to the left antenna (as in Fig. 1.4) introduces a time delay $\tau = (D/c)\sin\theta$, where D is the antenna spacing, θ is the angular position of the source, and c is the velocity of light. Thus, the signal from the left antenna is $V\sin[2\pi\nu_0(t-\tau)]$. The detector of the receiver generates a response proportional to the squared sum of the two signal voltages:

$$\{V\sin(2\pi\nu_0 t) + V\sin[2\pi\nu_0(t-\tau)]\}^2 \,. \tag{1.11}$$

The output of the detector is averaged in time, i.e., it contains a lowpass filter that removes any frequencies greater than a few hertz or tens of hertz, so in

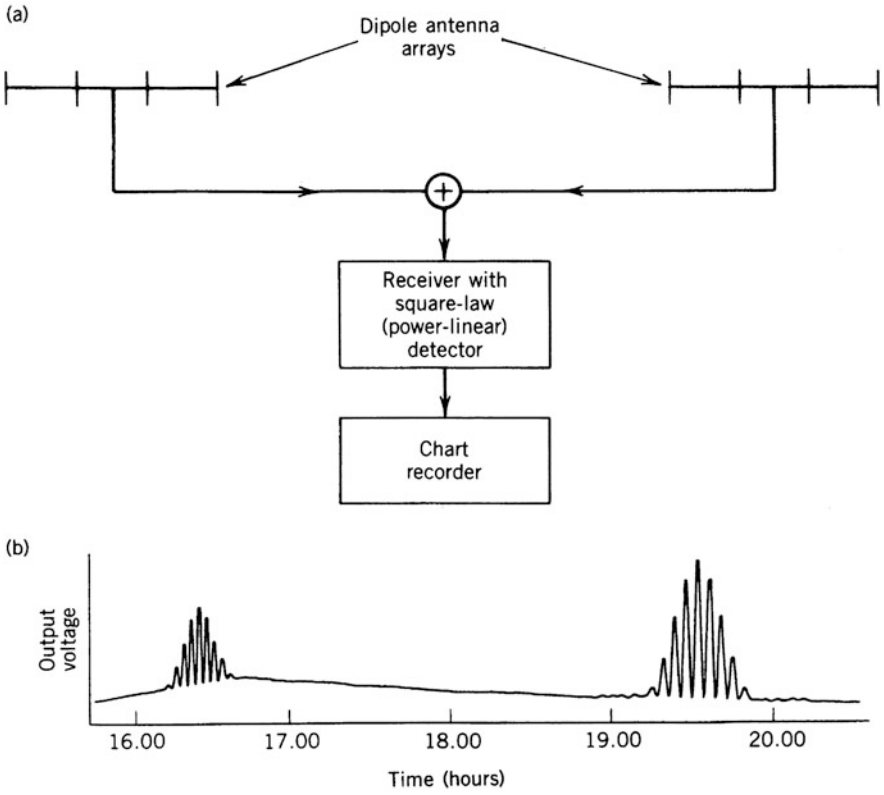

Fig. 1.6 (**a**) A simple interferometer, also called an adding interferometer, in which the signals are combined additively. (**b**) Record from such an interferometer with east–west antenna spacing. The ordinate is the total power received, since the voltage from the square-law detector is proportional to power, and the abscissa is time. The source at the left is Cygnus A and the one at the right Cassiopeia A. The increase in level near Cygnus A results from the galactic background radiation, which is concentrated toward the plane of our Galaxy but is completely resolved by the interferometer fringes. The record is from Ryle (1952). Reproduced with permission of the Royal Society, London, and the Master and Fellows of Churchill College, Cambridge. © Royal Society.

expanding (1.11), we can ignore the term in the harmonic of $2\pi\nu_0 t$. The detector output,[2] in terms of the power P_0 generated by either of the antennas alone, is therefore

$$P = P_0[1 + \cos(2\pi\nu_0\tau)] \,. \tag{1.12}$$

[2]For simplicity, in expression (1.11), we added the signal voltages from each antenna. In practice, such signals must be combined in networks that obey the conservation of power. Thus, if the signal from each antenna is represented as a voltage source V and characteristic impedance R, the power available is V^2/R. Combining two signals in series can be represented by a voltage $2V$ and impedance $2R$, giving a power of $2V^2/R$. In contrast, in free space, the addition of two coherent electric fields of equal strength quadruples the power. This distinction is important in the discussion of the sea interferometer (Sect. 1.3.4).

Because τ varies only slowly as the Earth rotates, the frequency represented by $\cos(2\pi\nu_0\tau)$ is not filtered out. In terms of the source position, θ, we have

$$P = P_0\left[1 + \cos\left(\frac{2\pi\nu_0 D\sin\theta}{c}\right)\right]. \tag{1.13}$$

Thus, as the source moves across the sky, P varies between 0 and $2P_0$, as shown by the sources in Fig. 1.6b. The response is modulated by the beam pattern of the antennas, of which the maximum is pointed in the meridian. The cosine function in Eq. (1.13) represents the Fourier component of the source brightness to which the interferometer responds. The angular width of the fringes is less than the angular width of the antenna beam by (approximately) the ratio of the width of an antenna to the baseline D, which in this example is about 1/10. The use of an interferometer instead of a single antenna results in a corresponding increase in precision in determining the time of transit of the source. The form of the fringe pattern in Eq. (1.13) also applies to the Michelson interferometer in Fig. 1.4. In the former case (radio), the fringes develop as a function of time, while in the latter case (optical), they appear as a function of position in the pupil plane of the telescope.

1.3.4 Sea Interferometer

A different implementation of interferometry, known as the sea interferometer, or Lloyd's mirror interferometer (Bolton and Slee 1953), was provided by a number of horizon-pointing antennas near Sydney, Australia. These had been installed for radar during World War II at several coastal locations, at elevations of 60–120 m above the sea. Radiation from sources rising over the eastern horizon was received both directly and by reflection from the sea, as shown in Fig. 1.7. The frequencies of the observations were in the range 40–400 MHz, the middle part of the range being the most satisfactory because of the sensitivity of receivers there and because of ionospheric effects at lower frequencies and sea roughness at higher frequencies. The sudden appearance of a rising source was useful in separating individual sources. Because of the reflected wave, the power received at the peak of a fringe was four times that for direct reception with the single antenna, and twice that of an adding interferometer with two of the same antennas (see footnote 2). Observations of the Sun by McCready et al. (1947) using this system provided the first published record of interference fringes in radio astronomy. They recognized that they were measuring a Fourier component of the brightness distribution and used the term "Fourier synthesis" to describe how an image could be produced from fringe visibility measurements on many baselines. Observations of the source Cygnus A by Bolton and Stanley (1948) provided the first positive evidence of the existence of a discrete nonsolar radio source. Thus, the sea interferometer played an important part in early radio astronomy, but the effects of the long atmospheric paths, the roughness of the sea surface, and the difficulty of varying the physical length of the baseline, which was set by the cliff height, precluded further useful development.

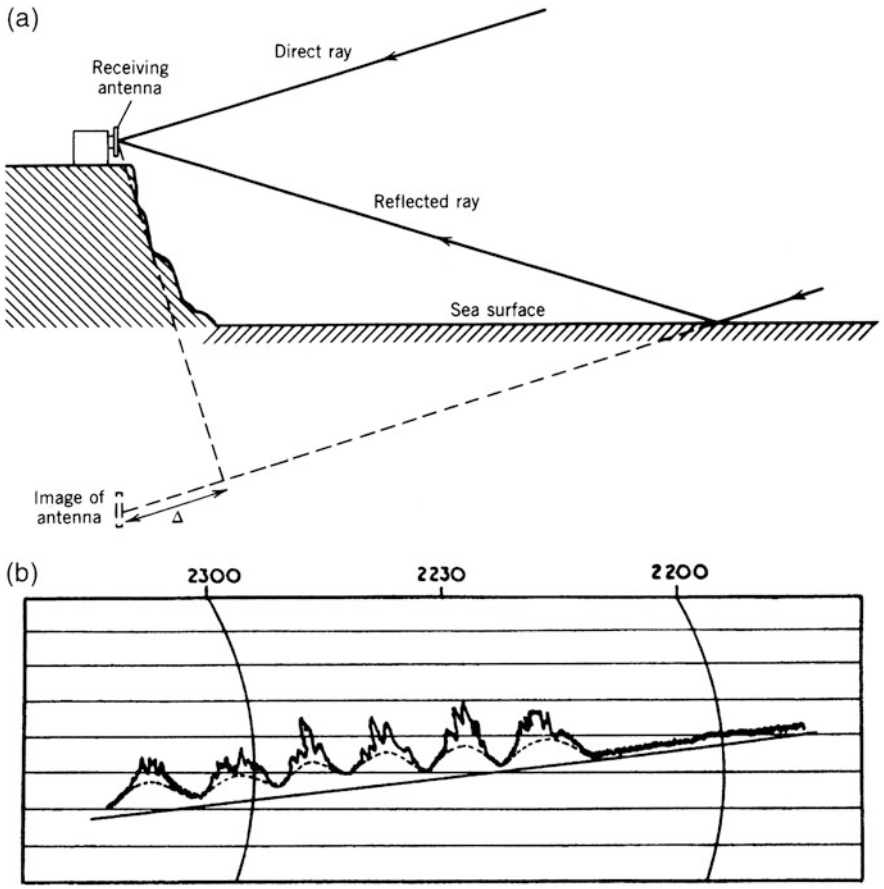

Fig. 1.7 (**a**) Schematic diagram of a sea interferometer. The fringe pattern is similar to that which would be obtained with the actual receiving antenna and one at the position of its image in the sea. The reflected ray undergoes a phase change of 180° on reflection and travels an extra distance Δ in reaching the receiving antenna. (**b**) Sea interferometer record of the source Cygnus A at 100 MHz by Bolton and Stanley (1948). The source rose above the horizon at approximately $22^{h}17^{m}$. The broken line was inserted to show that the record could be interpreted in terms of a steady component and a fluctuating component of the source; the fluctuations were later shown to be of ionospheric origin. The fringe width was approximately 1.0° and the source is unresolved, that is, its angular width is small in comparison with the fringe width. Part (**b**) is reprinted by permission from MacMillan Publishers Ltd.: *Nature*, **161**, 312–313, © 1948.

1.3.5 Phase-Switching Interferometer

A problem with the interferometer systems in both Figs. 1.6 and 1.7 is that in addition to the signal from the source, the output of the receiver contains components from other sources of noise power such as the galactic background radiation, thermal noise from the ground picked up in the antenna sidelobes, and

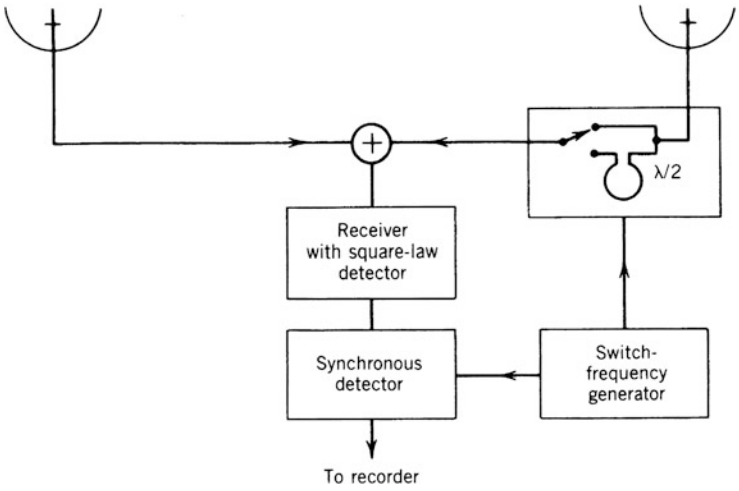

Fig. 1.8 Phase-switching interferometer. The signal from one antenna is periodically reversed in phase, indicated here by switching an additional half-wavelength of path into the transmission line.

the noise generated in the amplifiers of the receiver. For all except the few strongest cosmic sources, the component from the source is several orders of magnitude less than the total noise power in the receiver. Thus, a large offset has been removed from the records shown in Figs. 1.6b and 1.7b. This offset is proportional to the receiver gain, changes in which are difficult to eliminate entirely. The resulting drifts in the output level degrade the detectability of weak sources and the accuracy of measurement of the fringes. With the technology of the 1950s, the receiver output was usually recorded on a paper chart and could be lost when baseline drifts caused the recorder pen to go off scale.

The introduction of *phase switching* by Ryle (1952), which removed the unwanted components of the receiver output, leaving only the fringe oscillations, was the most important technical improvement in early radio interferometry. If V_1 and V_2 represent the signal voltages from the two antennas, the output from the simple adding interferometer is proportional to $(V_1 + V_2)^2$. In the phase-switching system, shown in Fig. 1.8, the phase of one of the signals is periodically reversed, so the output of the detector alternates between $(V_1 + V_2)^2$ and $(V_1 - V_2)^2$. The frequency of the switching is a few tens of hertz, and a synchronous detector takes the difference between the two output terms, which is proportional to $V_1 V_2$. Thus, the output of a phase-switching interferometer is the time average of the product of the signal voltages; that is, it is proportional to the cross-correlation of the two signals. The circuitry that performs the multiplication and averaging of the signals in a modern interferometer is known as a *correlator*: a more general definition of a correlator will be given later. Comparison with the output of the system in Fig. 1.6 shows that if the signals from the antennas are multiplied instead of added and squared, then the constant term within the square brackets in Eq. (1.13)

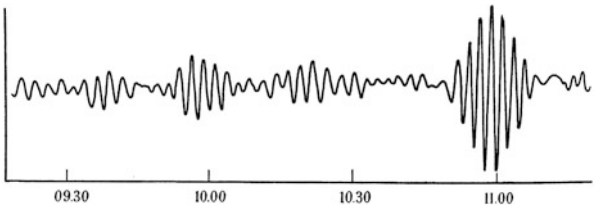

Fig. 1.9 Output of a phase-switching interferometer as a function of time, showing the response to a number of sources. From Ryle (1952). Reproduced with permission of the Royal Society, London, and the Master and Fellows of Churchill College, Cambridge. © Royal Society.

disappears, and only the cosine term remains. The output consists of the fringe oscillations only, as shown in Fig. 1.9. The removal of the constant term greatly reduces the sensitivity to instrumental gain variation, and it becomes practicable to install amplifiers at the antennas to overcome attenuation in the transmission lines. This advance resulted in the use of longer antenna spacings and larger arrays. Most interferometers from about 1950 onward incorporated phase switching, which provided the earliest means of implementing the multiplying action of a correlator. With more modern instruments, it is no longer necessary to use phase switching to obtain the voltage-multiplying action, but it is often included to help eliminate various instrumental imperfections, as described in Sect. 7.5.

1.3.6 Optical Identifications and Calibration Sources

Interferometer observations by Bolton and Stanley (1948), Ryle and Smith (1948), Ryle et al. (1950), and others provided evidence of numerous discrete sources. Identification of the optical counterparts of these required accurate measurement of radio positions. The principal method then in use for position measurement with interferometers was to determine the time of transit of the central fringe using an east–west baseline, and also the frequency of the fringe oscillations, which is proportional to the cosine of the declination (see Sect. 12.1 for more details). The measurement of position is only as accurate as the knowledge of the interferometer fringe pattern, which is determined by the relative locations of the electrical centers of the antennas. In addition, any inequality in the electrical path lengths in the cables and amplifiers from the antennas to the point where the signals are combined introduces an instrumental phase term, which offsets the fringe pattern. Smith (1952a) obtained positions for four sources with rms errors as small as $\pm 20''$ in right ascension and $\pm 40''$ in declination and gave a detailed analysis of the accuracy that was attainable. The optical identification of Cygnus A and Cassiopeia A by Baade and Minkowski (1954a,b) was a direct result of improved radio positions by Smith (1951) and Mills (1952). Cygnus A proved to be a distant galaxy and Cassiopeia A

a supernova remnant, but the interpretation of the optical observations was not fully understood at the time.

The need for absolute calibration of the antennas and receiving system rapidly disappeared after a number of compact radio sources were identified with optical objects. Optical positions accurate to $\sim 1''$ could then be used, and observations of such sources enabled calibration of interferometer baseline parameters and fringe phases. Although it cannot be assumed that the radio and optical positions of a source coincide exactly, the offsets for different sources are randomly oriented. Thus, errors were reduced as more calibration sources became available. Another important way of obtaining accurate radio positions during the 1960s and 1970s was by observation of occultation of sources by the Moon, which is described in Sect. 17.2.

1.3.7 Early Measurements of Angular Width

Comparison of the angular widths of radio sources with the corresponding dimensions of their optical counterparts helped in some cases to confirm identifications as well as to provide important data for physical understanding of the emission processes. In the simplest procedure, measurements of the fringe amplitude are interpreted in terms of intensity models such as those shown in Fig. 1.5. The peak-to-peak fringe amplitude for a given spacing normalized to the same quantity when the source is unresolved provides a measure of the fringe visibility equivalent to the definition in Eq. (1.9).

Some of the earliest measurements were made by Mills (1953), who used an interferometer operating at 101 MHz, in which a small transportable array of Yagi elements could be located at distances up to 10 km from a larger antenna. The signal from this remote antenna was transmitted back over a radio link, and fringes were formed. Smith (1952b,c), at Cambridge, England, also measured the variation of fringe amplitude with antenna spacing but used shorter baselines than Mills and concentrated on precise measurements of small changes in the fringe amplitude. Results by both investigators provided angular sizes of a number of the strongest sources: Cassiopeia A, the Crab Nebula, NGC4486 (Virgo A), and NGC5128 (Centaurus A).

A third early group working on angular widths at the Jodrell Bank Experimental Station,[3] England, used a different technique: *intensity interferometry* (Jennison and Das Gupta 1953, 1956; Jennison 1994). Hanbury Brown and Twiss (1954) had shown that if the signals received by two spaced antennas are passed through square-law detectors, the fluctuations in the intensity that result from the Gaussian fluctuations in the received field strength are correlated. The degree of correlation

[3]Later known as the Nuffield Radio Astronomy Laboratories, and since 1999 as the Jodrell Bank Observatory.

varies in proportion to the square of the visibility that would be obtained in a conventional interferometer in which signals are combined before detection. The intensity interferometer has the advantage that it is not necessary to preserve the radio-frequency phase of the signals in bringing them to the location at which they are combined. This simplifies the use of long baselines, which in this case extended up to 10 km. A VHF radio link was used to transmit the detected signal from the remote antenna, for measurement of the correlation. The disadvantage of the intensity interferometer is that it requires a high SNR, and even for Cygnus A and Cassiopeia A, the two highest flux-density sources in the sky, it was necessary to construct large arrays of dipoles, which operated at 125 MHz. The intensity interferometer is discussed further in Sect. 17.1, but it has been of only limited use in radio astronomy because of its lack of sensitivity.

The most important result of these intensity interferometer measurements was the discovery that for Cygnus A, the fringe visibility for the east–west intensity profile falls close to zero and then increases to a secondary maximum as the antenna spacing is increased. Two symmetric source models were consistent with the visibility values derived from the measurements. These were a two-component model in which the phase of the fringes changes by 180° in going through the minimum, and a three-component model in which the phase does not change. The intensity interferometer gives no information on the fringe phase, so a subsequent experiment was made by Jennison and Latham (1959) using conventional interferometry. Because the instrumental phase of the equipment was not stable enough to permit calibration, three antennas were used and three sets of fringes for the three pair combinations were recorded simultaneously. If ϕ_{mn} is the phase of the fringe pattern for antennas m and n, it is easy to show that at any instant, the combination

$$\phi_{123} = \phi_{12} + \phi_{23} + \phi_{31} \tag{1.14}$$

is independent of instrumental and atmospheric phase effects and is a measure of the corresponding combination of fringe phases (Jennison 1958). By moving one antenna at a time, it was found that the phase does indeed change by approximately 180° at the visibility minimum and therefore that the two-component model in Fig. 1.10 is the appropriate one. The use of combinations of simultaneous visibility measurements typified by Eq. (1.14), now referred to as *closure relationships*, became important about 20 years later in image-processing techniques. Closure relationships and the conditions under which they apply are discussed in Sect. 10.3. They are now integral parts of the self-calibration used in image formation (see Sect. 11.3).

The results on Cygnus A demonstrated that the simple models of Fig. 1.5 are not generally satisfactory for representation of radio sources. To determine even the most basic structure, it is necessary to measure the fringe visibility at spacings well beyond the first minimum of the visibility function to detect multiple components, and to make such measurements at a number of position angles across the source.

An early interferometer aimed at achieving high angular resolution with high sensitivity was developed by Hanbury Brown et al. (1955) at the Jodrell Bank

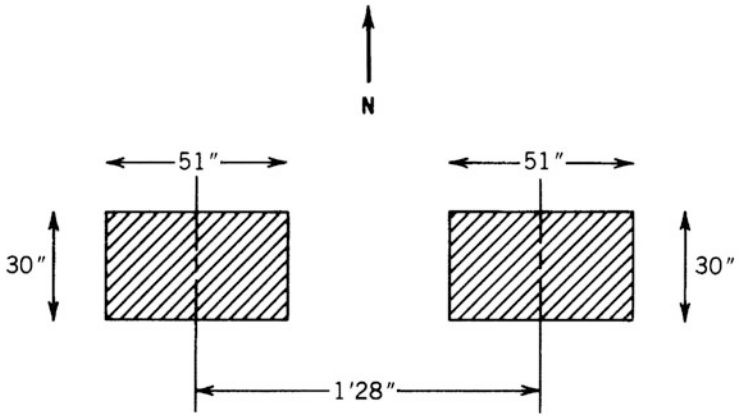

Fig. 1.10 Two-component model of Cygnus A derived by Jennison and Das Gupta (1953) using the intensity interferometer. Reprinted by permission from MacMillan Publishers Ltd.: *Nature*, **172**, 996–997, © 1953.

Experimental Station. This interferometer used an offset local oscillator technique at one antenna that took the place of a phase switch and also enabled the frequency of the fringe pattern to be slowed down to within the response time of the chart recorder used to record the output. A radio link was used to bring the signal from the distant antenna. Three sources were found to have diameters less than 12″ using spacings up to 20 km at 158 MHz observing frequency (Morris et al. 1957). During the 1960s, this instrument was extended to baselines of up to 134 km to achieve resolution of less than 1″ and greater sensitivity (Elgaroy et al. 1962; Adgie et al. 1965). The program later led to the development of a multielement, radio-linked interferometer known as the MERLIN array (Thomasson 1986).

1.3.8 Early Survey Interferometers and the Mills Cross

In the mid-1950s, the thrust of much work was toward cataloging larger numbers of sources with positions of sufficient accuracy to allow optical identification. The instruments operated mainly at meter wavelengths, where the spectrum was then much less heavily crowded with manmade emissions. A large interferometer at Cambridge used four antennas located at the corners of a rectangle 580 m east–west by 49 m north–south (Ryle and Hewish 1955). This arrangement provided both east–west and north–south fringe patterns for measurement of right ascension and declination.

A different type of survey instrument was developed by Mills et al. (1958) at Fleurs, near Sydney, consisting of two long, narrow antenna arrays in the form of a cross, as shown in Fig. 1.11. Each array produced a *fan beam*, that is, a beam that is narrow in a plane containing the long axis of the array and wide in the orthogonal

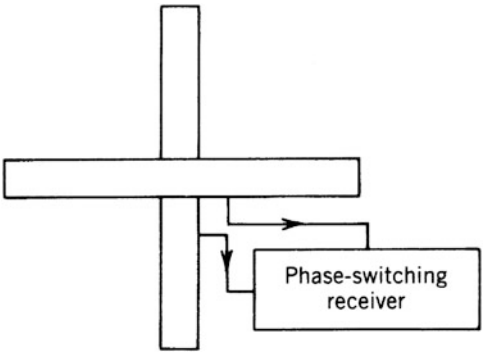

Fig. 1.11 Simplified diagram of the Mills cross radio telescope. The cross-shaped area represents the apertures of the two antennas.

direction. The outputs of these two arrays were combined in a phase-switching receiver, and the voltage-multiplying action produced a power-response pattern equal to the product of the voltage responses of the two arrays. This combined response had the form of a narrow *pencil beam*. The two arrays had a common electrical center, so there were no interferometer fringes. The arrays were 457 m long, and the cross produced a beam of width 49 arcmin and approximately circular cross section at 85.5 MHz. The beam pointed in the meridian and could be steered in elevation by adjusting the phase of the dipoles in the north–south arm. The sky survey made with this instrument provided a list of more than 2,200 sources.

A comparison of the source catalogs from the Mills cross with those from the Cambridge interferometer, which initially operated at 81.5 MHz (Shakeshaft et al. 1955), showed poor agreement between the source lists for a common area of sky (Mills and Slee 1957). The discrepancy was found to result principally from the occurrence of *source confusion* in the Cambridge observations. When two or more sources are simultaneously present within the antenna beams, they produce fringe oscillations with slightly different frequencies, resulting from differences in the source declinations. Maxima in the fringe amplitude, which occur when the fringe components happen to combine in phase, can mimic responses to sources. This was a serious problem because the beams of the interferometer antennas were too wide, a problem that did not arise in the Mills cross, which was designed to provide the required resolution for accurate positions in the single pencil beam. The frequency of the Cambridge interferometer was later increased to 159 MHz, thereby reducing the solid angles of the beams by a factor of four, and a new list of 471 sources was rapidly compiled (Edge et al. 1959). This was the 3C survey (source numbers, listed in order of right ascension, are preceded by 3C, indicating the third Cambridge catalog). The revised version of this survey (Bennett 1962, the 3C catalog) had 328 entries (some additions and deletions) and became a cornerstone of radio astronomy for the following decade. To avoid confusion problems and errors in flux-density distributions determined with these types of instruments as well as single-element telescopes, some astronomers subsequently recommended that the density of sources cataloged should not, on average, exceed 1 in roughly 20 times the solid angle of the resolution element of the measurement instrument (Pawsey

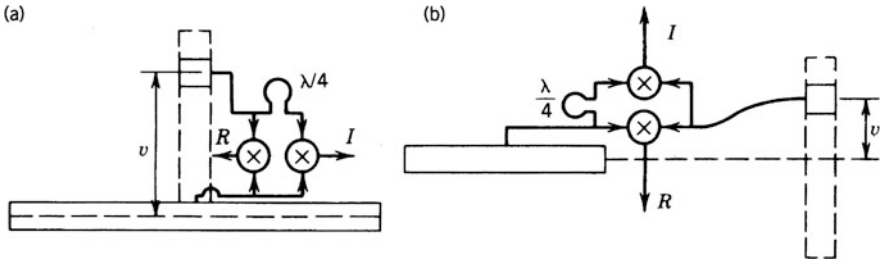

Fig. 1.12 Schematic diagrams of two instruments, in each of which a small antenna is moved to different positions between successive observations to synthesize the response that would be obtained with a full aperture corresponding to the rectangle shown by the broken line. The arrangement of two signal-multiplying correlators producing real (R) and imaginary (I) outputs is explained in Sect. 6.1.7. Instruments of both types, the T-shaped array (**a**), and the two-element interferometer (**b**), were constructed at the Mullard Radio Astronomy Observatory, Cambridge, England.

1958; Hazard and Walsh 1959). This criterion depends on the slope of a source count vs. flux density distribution (Scheuer 1957). For a modern treatment of the effects of source confusion, see Condon (1974) and Condon et al. (2012).

In the 1960s, a generation of new and larger survey instruments began to appear. Two such instruments developed at Cambridge are shown in Fig. 1.12. One was an interferometer with one antenna elongated in the east–west direction and the other north–south, and the other was a large T-shaped array that had characteristics similar to those of a cross, as explained in Sect. 5.3.3. In each of these instruments, the north–south element was not constructed in full, but the response with such an aperture was synthesized by using a small antenna that was moved in steps to cover the required aperture; a different position was used for each 24-h scan in right ascension (Ryle et al. 1959; Ryle and Hewish 1960). The records from the various positions were combined by computer to synthesize the response with the complete north–south aperture. An analysis of these instruments is given by Blythe (1957). The large interferometer produced the 4C (Fourth Cambridge) catalog containing over 4,800 sources (Gower et al. 1967). At Molonglo in Australia, a larger Mills cross (Mills et al. 1963) was constructed with arrays 1 mile long, producing a beam of 2.8-arcmin width at 408 MHz. The development of the Mills cross is described in papers by Mills and Little (1953), Mills (1963), and Mills et al. (1958, 1963). Crosses of comparable dimensions located in the Northern Hemisphere included one at Bologna, Italy (Braccesi et al. 1969), and one at Serpukhov, near Moscow in the former Soviet Union (Vitkevich and Kalachev 1966).

1.3.9 Centimeter-Wavelength Solar Imaging

A number of instruments have been designed specifically for imaging the Sun. The antennas were usually parabolic reflectors mounted to track the Sun, but since the

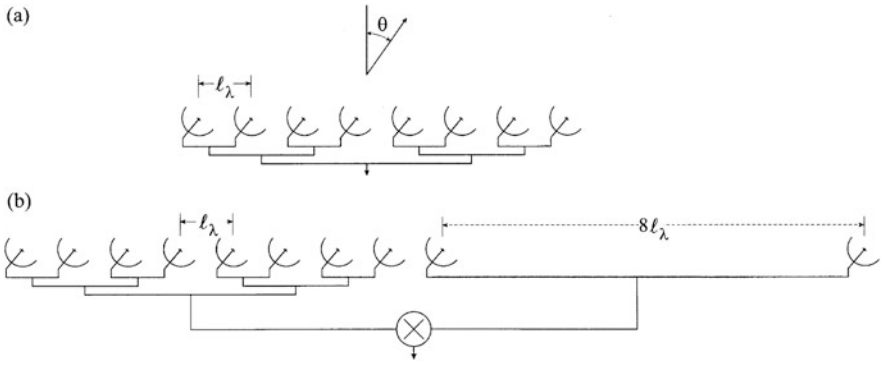

Fig. 1.13 (**a**) A linear array of eight equally spaced antennas connected by a branching network in which the electrical path lengths from the antennas to the receiver input are equal. This arrangement is sometimes referred to as a grating array, and in practice, there are usually 16 or more antennas. (**b**) An eight-element grating array combined with a two-element array to enhance the angular resolution. A phase-switching receiver, indicated by the multiplication symbol, is used to form the product of the signal voltages from the two arrays. The receiver output contains the simultaneous responses of antenna pairs with 16 different spacings. Systems of this general type were known as compound interferometers.

Sun is a strong radio source, the apertures did not have to be very large. Figure 1.13a shows an array of antennas from which the signals at the receiver input are aligned in phase when the angle θ between the direction of the source and a plane normal to the line of the array is such that $\ell_\lambda \sin\theta$ is an integer, where ℓ_λ is the unit antenna spacing measured in wavelengths. This type of array is sometimes referred to as a grating array, since it forms a series of fan-shaped beams, narrow in the θ direction, in a manner analogous to the response of an optical diffraction grating. It is useful only for solar observations in which all but one of the beams falls on "quiet" sky. Christiansen and Warburton (1955) obtained a two-dimensional image of the quiet Sun at 21-cm wavelength using both east–west and north–south grating arrays. These arrays consisted of 32 (east–west) and 16 (north–south) uniformly spaced, parabolic antennas. As the Sun moved through the sky, it was scanned at different angles by the different beams, and a two-dimensional map could be synthesized by Fourier analysis of the scan profiles. To obtain a sufficient range of scan angles, observations extending over eight months were used. In later instruments for solar imaging, it was generally necessary to be able to make a complete image within a day to study the variation of enhanced solar emission associated with active regions. Several instruments used grating arrays, typically containing 16 or 32 antennas and crossed in the manner of a Mills cross. Crossed grating arrays produce a rectangular matrix pattern of beams on the sky, and the rotation of the Earth enables sufficient scans to be obtained to provide daily maps of active regions and other features. Instruments of this type included crosses at 21-cm wavelength at Fleurs, Australia (Christiansen and Mullaly 1963), and at 10-cm wavelength at Stanford, California (Bracewell and Swarup 1961), and a T-shaped array at 1.9-m wavelength at Nançay,

France (Blum et al. 1957, 1961). These were the earliest imaging arrays with large numbers ($\sim$ 16 or more) of antennas.

Figure 1.13b illustrates the principle of a configuration known as a *compound interferometer* (Covington and Broten 1957), which was used to enhance the performance of a grating array or other antenna with high angular resolution in one dimension. The system shown consists of the combination of a grating array with a two-element array. An examination of Fig. 1.13b shows that pairs of antennas, chosen one from the grating array and one from the two-element array, can be found for all spacings from 1 to 16 times the unit spacing ℓ_λ. In comparison, the grating array alone provides only one to seven times the unit spacing, so the number of different spacings simultaneously contributing to the response is increased by a factor of more than two by the addition of two more antennas. Arrangements of this type were used to increase the angular resolution of one-dimensional scans of strong sources (Picken and Swarup 1964; Thompson and Krishnan 1965). By combining a grating array with a single larger antenna, it was also possible to reduce the number of grating responses on the sky (Labrum et al. 1963). Both the crossed grating arrays and the compound interferometers were originally operated with phase-switching receivers to combine the outputs of the two subarrays. In later implementations of similar systems, the signal from each antenna is converted to an intermediate frequency (IF), and a separate voltage-multiplying correlator was used for each spacing. This allows further possibilities in arranging the antennas to maximize the number of different antenna spacings, as discussed in Sect. 5.5.

1.3.10 Measurements of Intensity Profiles

Continuing measurements of the structure of radio sources indicated that in general, the intensity profiles are not symmetrical, so their Fourier transforms, and hence the visibility functions, are complex. This will be explained in detail in later chapters, but at this point, we note that it means that the phase of the fringe pattern (i.e., its position in time with respect to a fiducial reference), as well as the amplitude, varies with antenna spacing and must be measured to allow the intensity profiles to be recovered. To accommodate both fringe amplitude and phase, visibility is expressed as a complex quantity. Measurement of the fringe phase became possible in the 1960s and 1970s, by which time a number of compact sources with well-determined positions, suitable for calibration of the fringe phase, were available. Electronic phase stability had also improved, and computers were available for recording and processing the output data. Improvements in antennas and receivers enabled measurements to be made at wavelengths in the centimeter range (frequencies greater than $\sim$ 1 GHz), using tracking antennas.

An interferometer at the Owens Valley Radio Observatory, California (Read 1961), provides a good example of one of the earliest instruments used extensively for determining radio structure. It consisted of two 27.5-m-diameter parabolic antennas on equatorial mounts with a rail track system that allowed the spacing

between them to be varied by up to 490 m in both the east–west and north–south directions. It was used mainly at frequencies from 960 MHz to a few GHz. Studies by Maltby and Moffet (1962) and Fomalont (1968) illustrate the use of this instrument for measurement of intensity distributions, an example of which is shown in Fig. 1.14. Lequeux (1962) studied the structure of about 40 extragalactic sources at 1400 MHz on a reconfigurable two-element interferometer with baselines up to 1460 m (east–west) and 380 m (north–south) at Nançay Observatory in France. These are early examples of model fitting of visibility data, a technique of continuing usefulness (see Sect. 10.4).

1.3.11 Spectral Line Interferometry

The earliest spectral line measurements were made with single narrowband filters. By the early 1960s, the interferometer at Owens Valley and several others had been fitted with spectral line receiving systems. The passband of each receiver was divided into a number of channels by a filter bank, usually in the IF stages, and for each channel, the signals from the two antennas went to a separate correlator. In later systems, the IF signals were digitized and the filtering was performed digitally, as described in Sect. 8.8. The width of the channels should ideally be less than that of the line to be observed so that the line profile can be studied. Spectral line interferometry allows the distribution of the line emission across a radio source to be examined. Roger et al. (1973) describe an array in Canada built specifically for observations in the 1420 MHz (21-cm wavelength) line of neutral hydrogen.

Spectral lines can also be observed in absorption, especially in the case of the neutral hydrogen line. At the line frequency, the gas absorbs the continuum radiation from any more distant source that is observed through it. Comparison of the emission and absorption spectra of neutral hydrogen yields information on its temperature and density. Measurement of absorption spectra of sources can be made using single antennas, but in such cases, the antenna also responds to the broadly distributed emitting gas within the antenna beam. The absorption spectra for weak sources are difficult to separate from the line emission. With an interferometer, the broad emission features on the sky are almost entirely resolved and the narrow absorption spectrum can be observed directly. For early examples of hydrogen line absorption measurements, see Clark et al. (1962) and Hughes et al. (1971).

1.3.12 Earth-Rotation Synthesis Imaging

A very important step in the development of synthesis imaging was the use of the variation of the antenna baseline provided by the rotation of the Earth. Figure 1.15 illustrates this principle, as described by Ryle (1962). For a source at a high declination, the position angle of the baseline projected onto a plane normal to the

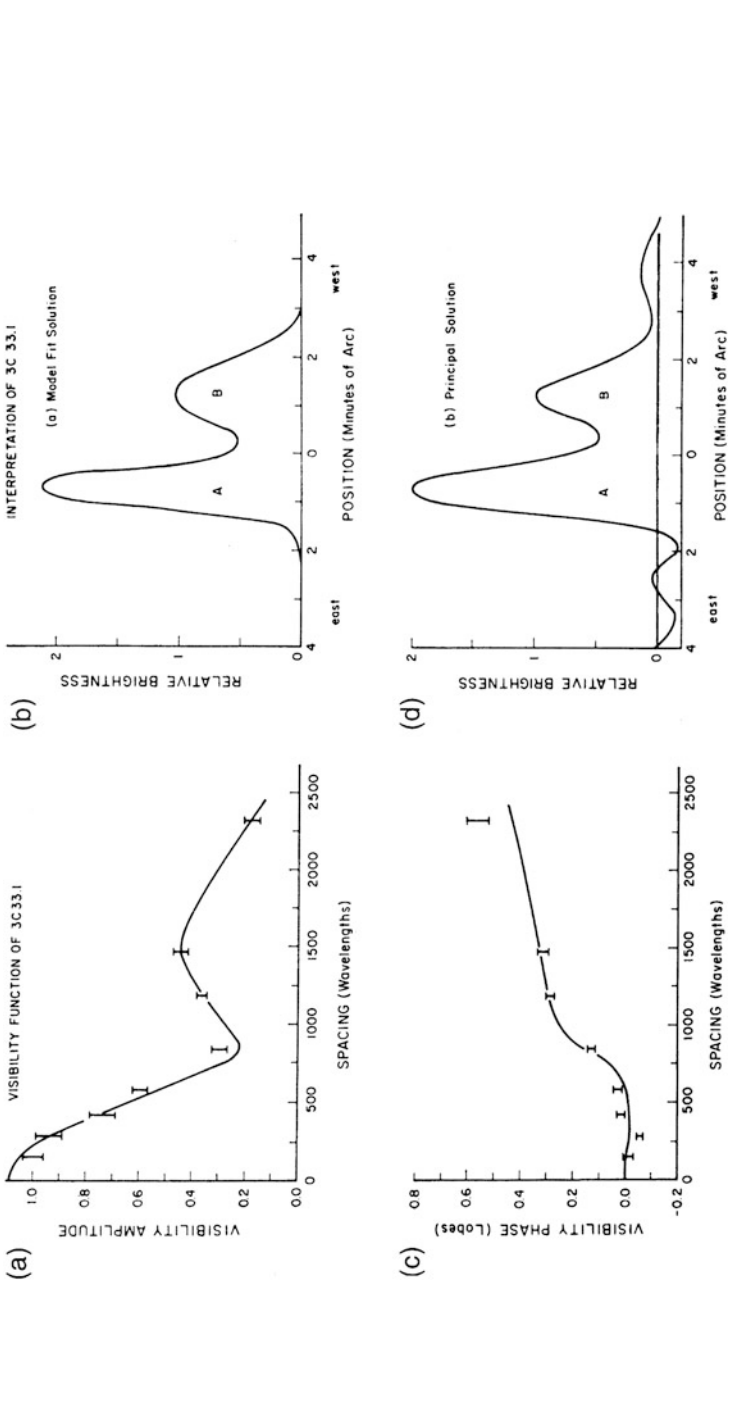

Fig. 1.14 Example of interferometer measurements of one-dimensional intensity (brightness): the east–west profile of source 3C33.1 as determined by Fomalont (1968) using the interferometer at the Owens Valley Radio Observatory at 1425 MHz. (**a**,**c**) The points show the measured amplitude and phase of the visibility. (**b**) The profile was obtained by fitting Gaussian components to the visibility data, as shown by the curves through the measured visibility points. (**d**) The profile was obtained by Fourier transformation of the observed visibility values. The unit of visibility phase (lobe) is 2π radians. From Fomalont (1968). © AAS. Reproduced by permission.

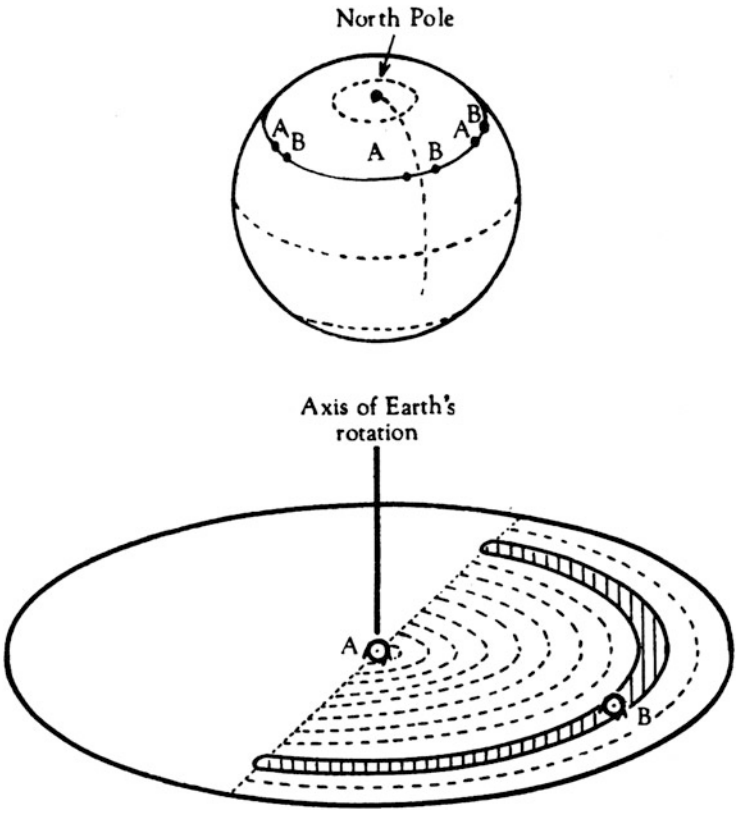

Fig. 1.15 Use of Earth rotation in synthesis imaging, as explained by Ryle (1962). The antennas A and B are spaced on an east–west line. By varying the distance between the antennas from one day to another, and observing for 12 h with each configuration, it is possible to encompass all the spacings from the origin to the elliptical outer boundary of the lower diagram. Only 12 h of observing at each spacing is required, since during the other 12 h, the spacings covered are identical but the positions of the antennas are effectively interchanged. Reprinted by permission from MacMillan Publishers Ltd.: *Nature*, **194**, 517–518, © 1962.

direction of the source rotates through 180° in 12 h. Thus, if the source is tracked across the sky for a series of 12-h periods, each one with a different antenna spacing, the required two-dimensional visibility data can be collected while the antenna spacing is varied in one dimension only. Calculation of two-dimensional Fourier transforms was an arduous task at this time.

The Cambridge One-Mile Radio Telescope was the first instrument designed to exploit fully the Earth-rotation technique and apply it to a large number of radio sources. The use of Earth rotation was not a sudden development in radio astronomy and had been used in solar studies for a number of years. O'Brien (1953) made two-dimensional Fourier synthesis observations with a movable-element interferometer, and, as noted earlier, Christiansen and Warburton (1955) had obtained a two-

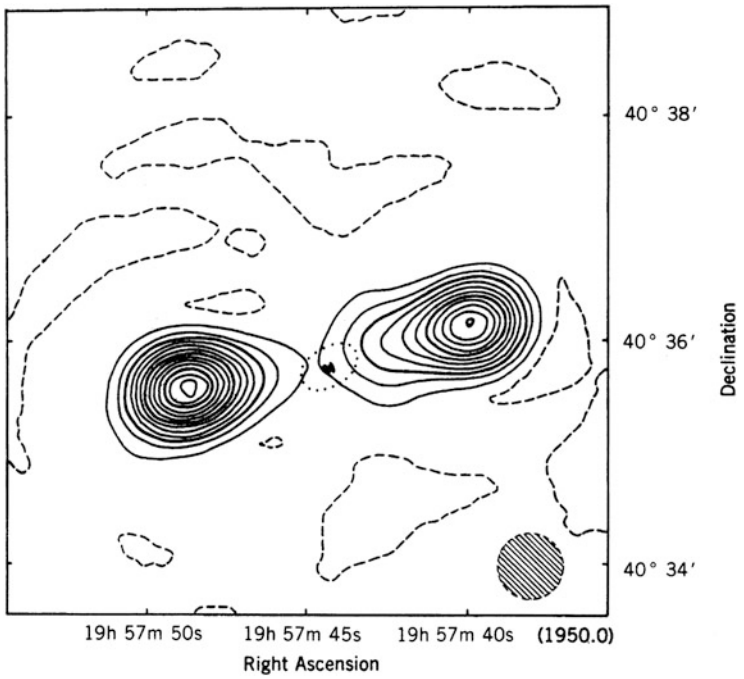

Fig. 1.16 Contour image of the source Cygnus A, which was one of the first results (Ryle et al. 1965) from the Cambridge One-Mile Telescope using the Earth-rotation principle shown in Fig. 1.15. The frequency is 1.4 GHz. The image has been scaled in declination so that the half-power beam contour is circular, as shown by the shaded area in the lower right corner. The dotted ellipse shows the outer boundary of the optical source, and its central structure is also indicated. Reprinted by permission from MacMillan Publishers Ltd.: *Nature*, **205**, 1259–1262, © 1965.

dimensional map of the Sun, using tracking antennas in two grating arrays. At Jodrell Bank, Rowson (1963) had used a two-element interferometer with tracking antennas to map strong nonsolar sources. Also, Ryle and Neville (1962) had imaged the north polar region using Earth rotation to demonstrate the technique. However, the first images published from the Cambridge One-Mile telescope, those of the strong sources Cassiopeia A and Cygnus A (Ryle et al. 1965), exhibited a degree of structural detail unprecedented in earlier studies and heralded the development of synthesis imaging. The image of Cygnus A is shown in Fig. 1.16.

1.3.13 Development of Synthesis Arrays

Following the success of the Cambridge One-Mile Telescope, interferometers such as the NRAO instrument at Green Bank, West Virginia (Hogg et al. 1969), were rapidly adapted for synthesis imaging. Several large arrays designed to provide increased imaging speed, sensitivity, and angular resolution were brought into

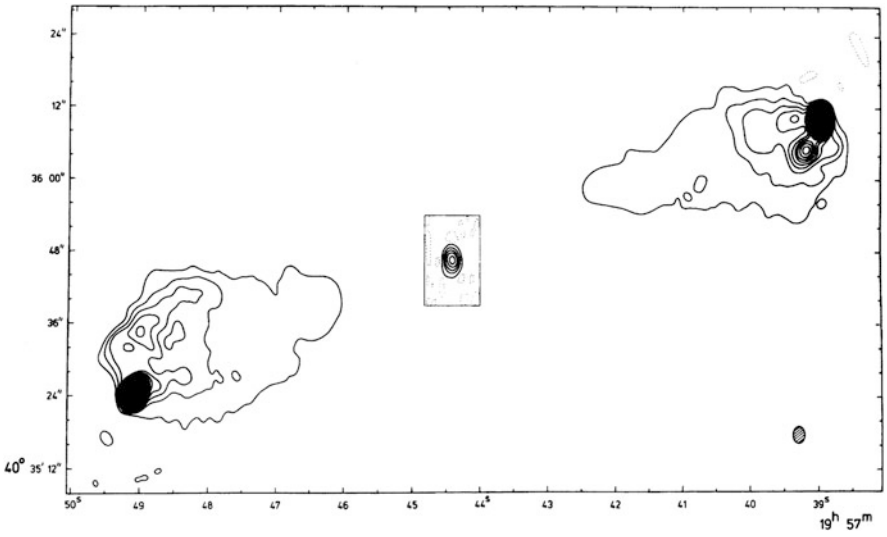

Fig. 1.17 Contour image of the source Cygnus A using the Cambridge Five-Kilometre Radio Telescope at 5 GHz. This showed for the first time the radio nucleus associated with the central galaxy and the high intensity at the outer edges of the radio lobes. From Hargrave and Ryle (1974). © Royal Astronomical Society, used with permission.

operation during the 1970s. Prominent among these were the Five-Kilometre Radio Telescope at Cambridge, England (Ryle 1972), the Westerbork Synthesis Radio Telescope in the Netherlands (Baars et al. 1973), and the Very Large Array (VLA) in New Mexico (Thompson et al. 1980; Napier et al. 1983). With these instruments, imaging of radio sources with a resolution of less than $1''$ at centimeter wavelengths was possible. By using n_a antennas, as many as $n_a(n_a-1)/2$ simultaneous baselines can be obtained. If the array is designed to avoid redundancy in the antenna spacings, the speed with which the visibility function is measured is approximately proportional to n_a^2. Images of Cygnus A obtained with two of the arrays mentioned above are shown in Figs. 1.17 and 1.18. Resolution of the central source was first achieved with very-long-baseline interferometry (VLBI, see Sect. 1.3.14) (Linfield 1981). A more recent VLBI image is shown in Fig. 1.19. A review of the development of synthesis instruments at Cambridge is given in the Nobel lecture by Ryle (1975). An array with large collecting area, the Giant Metrewave Radio Telescope (GMRT), which operates at frequencies from 38 to 1420 MHz, was completed in 1998 near Pune, India (Swarup et al. 1991). More recently, advances in broadband antenna technology and large-scale integrated circuits have enabled further large increases in performance. For example, the capability of the VLA was greatly improved with an updated electronic system (Perley et al. 2009).[4]

[4]The upgraded VLA was formally rededicated as the Karl G. Jansky Very Large Array and is sometimes referred to as the JVLA.

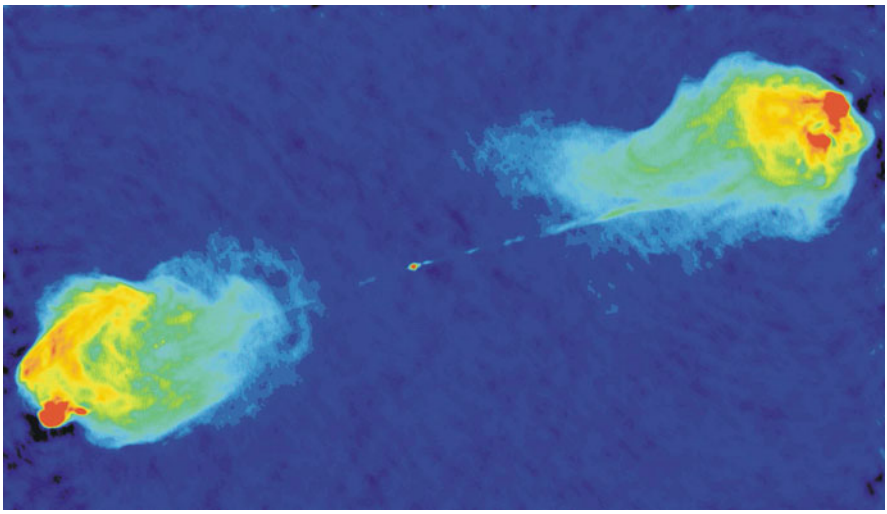

Fig. 1.18 Image of Cygnus A made with the VLA at 4.9 GHz. Observations with four configurations of the array were combined, and the resolution is $0.4''$. The display of the image shown here involves a nonlinear process to enhance the contrast of the fine structure. This emphasizes the jet from the central galaxy to the northwestern lobe (top right) and the filamentary structure in the main lobes. Comparison with other records of Cygnus A in this chapter illustrates the technical advances made during three decades. Reproduced by permission of NRAO/AUI. From Perley et al. (1984). © AAS. Reproduced with permission.

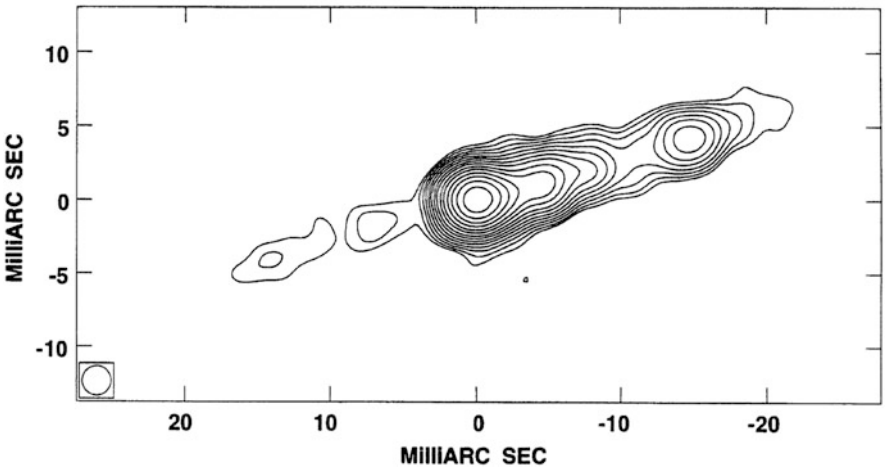

Fig. 1.19 VLBI image of the central part of Cygnus A at 5 GHz, imaged with a ten-station global VLBI array. The resolution is 2 mas, and the rms noise level is 0.4 mJy/beam. The coordinates are centered on the core components. The knots in the jet have apparent expansion speeds of ~ 0.4 c. The counter jet to the left of the core is clearly visible. The jet structure is more clearly defined in an image at 43 GHz with a resolution of 0.15 mas by Boccardi et al. (2016). From Carilli et al. (1994). © AAS. Reproduced with permission.

During the 1980s and 1990s, synthesis arrays operating at short millimeter wavelengths (frequencies of 100 GHz or greater) were developed. Spectral lines are particularly numerous at these frequencies (see Fig. 1.2). Several considerations are more important at millimeter wavelengths than at centimeter wavelengths. Because the wavelengths are much shorter, any irregularity in the atmospheric path length results in a proportionately greater effect on the signal phase. Attenuation in the neutral atmosphere is much more serious at millimeter wavelengths. Also, the beams of the individual antennas become narrower at shorter wavelengths, and maintenance of a sufficiently wide field of view is one reason why the antenna diameter tends to decrease with increasing frequency. Thus, to obtain the necessary sensitivity, larger numbers of antennas are required than at centimeter wavelengths. Arrays for millimeter wavelengths have included those at Hat Creek, California (Welch 1994); Owens Valley, California (Scoville et al. 1994)[5]; Nobeyama, Japan (Morita 1994); the Plateau de Bure, France (Guilloteau 1994); and Mauna Kea, Hawaii (Ho et al. 2004). The largest such array, the Atacama Large Millimeter/submillimeter Array (ALMA) consists of 50 12-m-diameter antennas in one array and 12 7-m-diameter antennas in another. Located in the Atacama Desert of Chile, a dry site at $\sim 5,000$-m elevation, its operating frequency range is 31–950 GHz, and antenna spacings range up to 14 km. The field of view, defined by the beamwidths of the antennas, is only about $8''$ at 345 GHz in the primary array. It is an international facility and came into operation in 2013 (Wootten and Thompson 2009).

1.3.14 Very-Long-Baseline Interferometry

Investigation of the angular diameters of quasars and other objects that appear nearly pointlike in structure presented an important challenge throughout the early years of radio astronomy. An advance that led to an immediate increase of an order of magnitude in resolution, and subsequently to several orders more, was the use of independent local oscillators and signal recorders. By using local oscillators at each antenna that are controlled by high-precision frequency standards, it is possible to preserve the coherence of the signals for time intervals long enough to measure interference fringes. In the early years, the received signals were converted to an intermediate frequency low enough that they could be recorded directly on magnetic tape and then brought together and played into a correlator. This technique became known as very-long-baseline interferometry (VLBI), and the early history of its development is discussed by Broten (1988), Kellermann and Cohen (1988), Moran (1998), and Kellermann and Moran (2001). The technical requirements for VLBI were discussed in the USSR in the early 1960s (see, e.g., Matveenko et al. 1965).

A successful early experiment was performed in January 1967 by a group at the University of Florida, who detected fringes from the burst radiation of Jupiter at

[5]The arrays at Hat Creek and Owens Valley were combined at Cedar Flats, a high site east of Owens Valley, to form the CARMA array, which operated from 2005 to 2015.

18 MHz (Brown et al. 1968). Because of the strong signals and low frequency, the required recording bandwidth was only 2 kHz and the frequency standards were crystal oscillators. Much more sensitive and precise VLBI systems, which used wider bandwidths and atomic frequency standards, were developed by three other groups. In Canada, an analog recording system was developed with a bandwidth of 1 MHz based on television tape recorders (Broten et al. 1967). Fringes were obtained at a frequency of 448 MHz on baselines of 183 and 3074 km on several quasars in April 1967. In the United States, another group from the National Radio Astronomy Observatory and Cornell University developed a computer-compatible digital recording system with a bandwidth of 360 kHz (Bare et al. 1967). They obtained fringes at 610 MHz on a baseline of 220 km on several quasars in May 1967. A third group from MIT joined in the development of the NRAO–Cornell system in early 1967 and obtained fringes at a frequency of 1665 MHz on a baseline of 845 km on several OH-line masers, with spectroscopic analysis, in June 1967 (Moran et al. 1967).

The initial experiments used signal bandwidths of less than a megahertz, but by the 1980s, systems capable of recording signals with bandwidths greater than 100 MHz were available, with corresponding improvements in sensitivity. Real-time linking of the signals from remote telescopes to the correlator via a geostationary satellite was demonstrated (Yen et al. 1977). Also, experiments were performed in which the local oscillator signal was distributed over a satellite link (Knowles et al. 1982). Neither of these satellite-supported techniques have been used significantly for practical and economic reasons. Most importantly, the accessibility of the world-wide network of fiberoptic transmission lines, which have since become available, allows real-time transmission of the data to the correlator. These developments, as well as the advent of sophisticated data analysis techniques, have lessened the distinction between VLBI and more conventional forms of interferometry. A detailed technical description of issues specific to the VLBI technique is given in Chap. 9.

An early example of the extremely high angular resolution that can be achieved with VLBI is provided by a measurement by Burke et al. (1972), who obtained a resolution of 200 μas using antennas in Westford, Massachusetts, and near Yalta in the Crimea, operating at a wavelength of 1.3 cm. Early measurements, obtained using a few baselines only, were generally interpreted in terms of the simple models in Fig. 1.5. Important results were the discovery and investigation of superluminal (apparently faster-than-light) motions in quasars (Whitney et al. 1971; Cohen et al. 1971), as shown in Fig. 1.20, and the measurement of proper motion in H_2O line masers (Genzel et al. 1981). During the mid-1970s, several groups of astronomers began to combine their facilities to obtain measurements over ten or more baselines simultaneously. In the United States, the Network Users' Group, later called the U.S. VLBI Consortium, included the following observatories: Haystack Observatory in Massachusetts (NEROC); Green Bank, West Virginia (NRAO); Vermilion River Observatory in Illinois (Univ. of Illinois); North Liberty in Iowa (Univ. of Iowa); Fort Davis, Texas (Harvard College Observatory); Hat Creek Observatory, California (Univ. of California); and Owens Valley Radio Observatory, California. Other

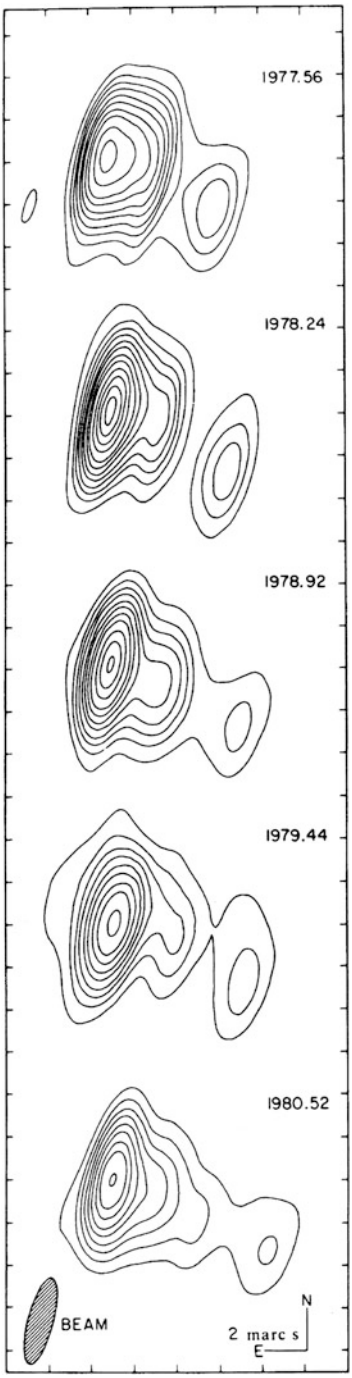

Fig. 1.20 VLBI images of the quasar 3C273 at five epochs, showing the relative positions of two components. From the distance of the object, deduced from the optical redshift, the apparent relative velocity of the components exceeds the velocity of light, but this can be explained by relativistic and geometric effects. The observing frequency is 10.65 GHz. An angular scale of 2 mas is shown in the lower right corner. From Pearson et al. (1981). Reprinted by permission from MacMillan Publishers Ltd.: *Nature*, **290**, 365–368, © 1981.

arrays, such as the European VLBI Network (EVN) soon developed. Observations on such networks led to more complex models [see, e.g., Cohen et al. (1975)].

A problem in VLBI observations is that the use of nonsynchronized local oscillators complicates the calibration of the phase of the fringes. It became evident early on that VLBI represented an intermediate form of interferometer between the intensity interferometer and the perfectly stable coherent interferometer (Clark 1968). Techniques were developed to combine coherent averaging on timescales up to a defined coherence time, followed by incoherent averaging. These techniques remain useful in VLBI at very high frequencies. To overcome the problem of calibration of phase for coherently averaged data, the phase closure relationship of Eq. (1.14) was first applied to VLBI data by Rogers et al. (1974). The technique rapidly developed into a method to obtain images known as hybrid mapping. For examples of hybrid mapping, see Figs. 1.19 and 1.20. This method was subsumed into the more general approach called self-calibration (see Chap. 11). For some spectral line observations in which the source consists of spatially isolated masers, the signals from which can be separated by their individual Doppler shifts, phase referencing techniques can be used (e.g., Reid et al. 1980).

The first array of antennas built specifically for astronomical measurements by VLBI, the Very Long Baseline Array (VLBA) of the U.S. National Radio Astronomy Observatory (NRAO), was brought into operation in 1994. It consists of ten 25-m-diameter antennas, one in the U.S. Virgin Islands, eight in the continental United States, and one in Hawaii (Napier et al. 1994). The VLBA is often linked with additional antennas to further improve the baseline coverage and sensitivity. Figure 1.21 presents a result from the combined VLBA and EVN array.

The great potential of VLBI in astrometry and geodesy was immediately recognized after the initial experiments in 1967 [see, e.g., Gold (1967)]. A seminal meeting defining the role of VLBI in Earth dynamics programs was held in Williamstown, Massachusetts, in 1969 (Kaula 1970). The use of VLBI in these applications developed rapidly during the 1970s and 1980s; see, for example, Whitney et al. (1976) and Clark et al. (1985). In the United States, NASA and several other federal agencies set up a cooperative program of geodetic measurements in the mid-1970s. This work evolved in part from the use of the Jet Propulsion Laboratory deep-space communications facilities for VLBI observations. It has expanded into an enormous worldwide effort carried out under the aegis of the International VLBI Service (IVS) and a network of more than 40 antennas. An important result of this effort has been the establishment of the International Celestial Reference Frame adopted by the IAU, which is based on 295 "defining" sources whose positions are known to an accuracy of about 40 μas (Fey et al. 2015). Another striking result of the geodetic VLBI work has been the detection of contemporary plate motions in the Earth's mantle, first measured as a change in the Westford–Onsala baseline at a rate of 17 ± 2 mm/yr (Herring et al. 1986). The VLBI measurements of plate motions is shown in Fig. 1.22. Astrometry with submilliarcsecond accuracy has opened up new possibilities in astronomy, for example, the detection of the motion of the Sun around the Galactic center from the proper motion of Sagittarius A* (Backer and Sramek 1999; Reid and Brunthaler 2004) and measurements of the

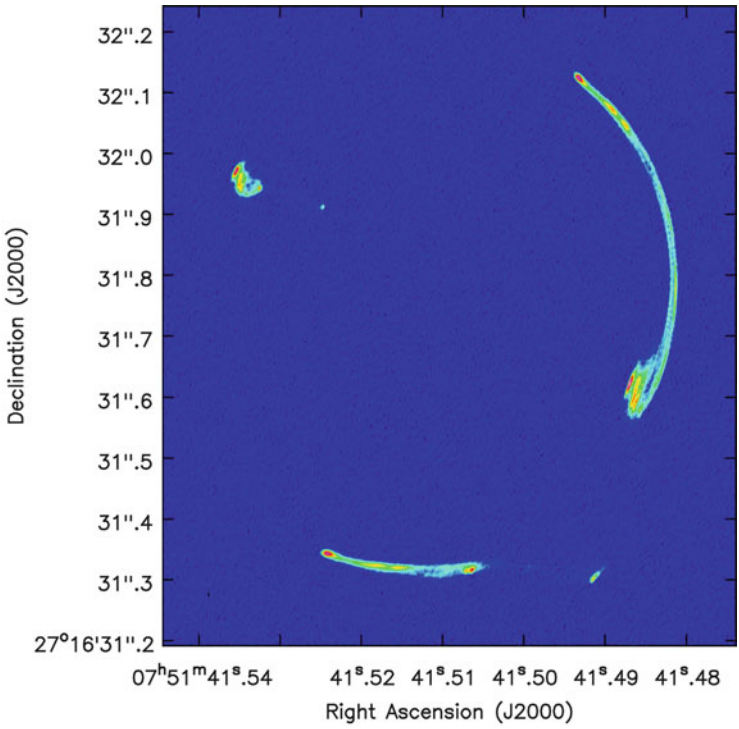

Fig. 1.21 Image of the gravitational lens source MG J0751+2716 made with a 14-h observation on a 21-element global VLBI Array (VLBA and the EVN plus the Green Bank telescope) at a frequency of 1.7 GHz. The rms noise level is 12 μJy, and the resolution is 2.2 × 5.6 mas. This image of an extended background source at redshift 3.2 is highly distorted by an unseen foreground radio-quiet galaxy at a redshift of 0.35 into extended arcs. Image courtesy of and © John McKean.

annual parallaxes of galactic radio sources (Reid and Honma 2014). Astrometric and geodetic methods are described in Chap. 12.

The combination of VLBI with spectral line processing is particularly effective in the study of problems that involve both astrometry and dynamical analysis of astronomical systems. The galaxy NGC4258, which exhibits an active galactic nucleus, has been found to contain a number of small regions that emit strongly in the 22.235-GHz water line as a result of maser processes. VLBI observations have provided an angular resolution of 200 μas, an accuracy of a few microarcseconds in the relative positions of the masers, and measurements of Doppler shifts to an accuracy of 0.1 km s^{-1} in radial velocity (see Fig. 1.23). NGC4258 is fortuitously aligned so that the disk is almost edge-on as viewed from the Earth. The orbital velocities of the masers, which obey Kepler's law, are accurately determined as a function of radius from the center of motion. Hence, the distance can be found by comparing the linear and angular motions. The angular motions are about 30 μas per year. These results provide a value for the central mass of 3.9 × 10^7 times

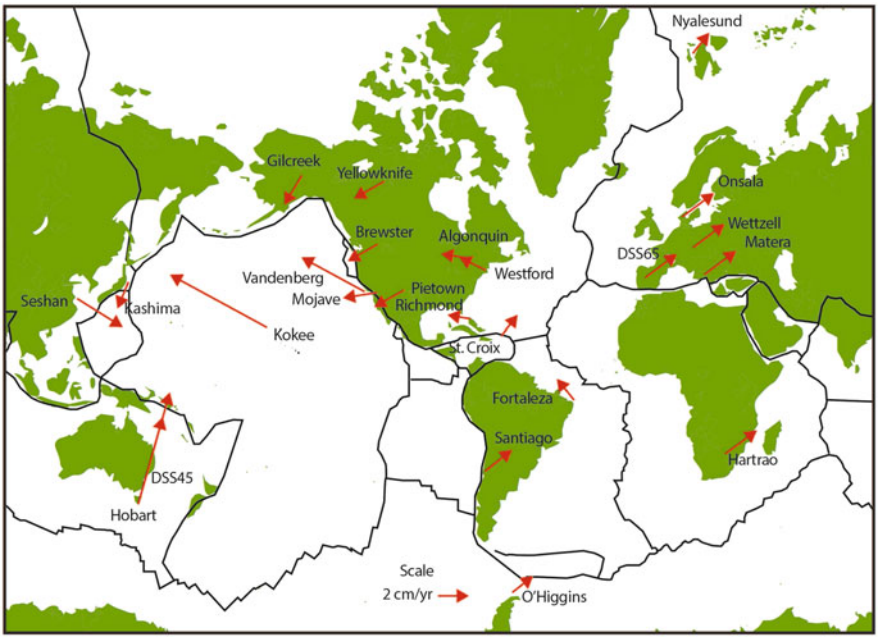

Fig. 1.22 Tectonic plate motions measured with VLBI. A VLBI station is located at the foot of each vector and labeled by the station name. The sum of the motion vectors is constrained to be zero. The largest motion is for the Kokee site in Hawaii, about 8 cm yr^{-1}. Plate boundaries, established by other techniques, are shown by the jagged lines. From Whitney et al. (2014). Reprinted with permission courtesy of and © MIT Lincoln Laboratory, Lexington, MA.

the mass of the Sun, presumably a supermassive black hole (Miyoshi et al. 1995; Herrnstein et al. 1999), and 7.6 ± 0.2 Mpc for the distance (Humphreys et al. 2013). The uncertainty of 3% in the distance of an extragalactic object, measured directly, set a precedent.

1.3.15 VLBI Using Orbiting Antennas

The use of spaceborne antennas in VLBI observations is referred to as the OVLBI (orbiting VLBI) technique. The first observations of this type were made in 1986 using a satellite of the U.S. Tracking and Data Relay Satellite System (TDRSS). These satellites were in geostationary orbit at a height of approximately 36,000 km and were used to relay data from low-Earth-orbit spacecraft to Earth. They carried two 4.9-m antennas used to communicate with other satellites at 2.3 and 15 GHz and a smaller antenna for the space-to-Earth link. In this experiment, one of the 4.9-m antennas was used to observe a radio source, and the other received a reference signal from a hydrogen maser on the ground (Levy et al. 1989). The received signals

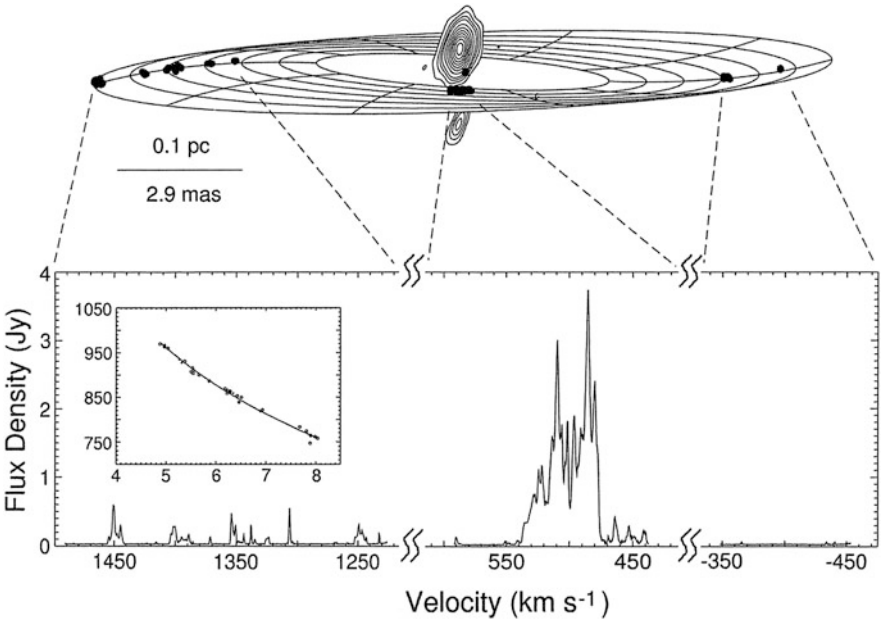

Fig. 1.23 Image of the water vapor maser disk in the core of the galaxy NGC4258 at 1.35 cm made with the VLBA. The spots mark the positions of the unresolved maser components. The elliptical grid lines denote the thin, slightly warped disk that the masers trace. The position of the gravitational center is shown by the black square. The contour plot shows the continuum emission from the central active galactic nucleus. Each maser spot corresponds to a feature in the spectrum in the lower panel. The strongest feature, at 470 km s^{-1}, serves as a phase reference. The inset shows the radial velocity of the masers vs. radial distance from the black hole in milliarcseconds. From Herrnstein et al. (2005). © AAS. Reproduced with permission.

were transmitted to the ground and recorded on a VLBI tape system for correlation with signals from ground-based antennas. The numbers of sources detected were 23 and 11 at 2.3 and 15 GHz, respectively (Linfield et al. 1989, 1990). At 15 GHz, the fringe width was of order 0.3 mas, and interpretation of the results in terms of circular Gaussian models indicated brightness temperatures as high as 2×10^{12} K.

VLBI observations using a satellite in a non-geostationary orbit were first made in 1997 by the VLBI Space Observatory Programme (VSOP) (Hirabayashi et al. 1998), designed specifically for VLBI observations. It was equipped with an antenna of 8-m diameter, and observations were made at 1.6 and 5 GHz. The orbital period was approximately 6.6 h and the apogee height, 21,000 km. VSOP was followed by the RadioAstron satellite, which was launched in 2011 into an orbit with an apogee height of about 300,000 km and a period of 8.3 days (Kardashev et al. 2013). It is equipped with an antenna of 10-m diameter and receivers at 18, 6, and 1.35 cm. Operating with ground-based telescopes, it can attain a resolution of 8 μas at 1.35 cm. More information about satellite VLBI can be found in Sect. 9.10.

The possibility of achieving very long baselines by reflection from the Moon has been discussed by Hagfors et al. (1990). Reflection from the surface of the Moon could provide baselines up to a length approaching the radius of the lunar orbit. An antenna of 100-m aperture, or larger, would be used to track the Moon and receive the reflected signal from the source under study, and a smaller antenna could be used for the direct signal. It is estimated that the sensitivity would be about three orders of magnitude less than would be obtained by observing the source directly with both antennas. Further complications result from the roughness of the lunar surface and from libration. The technique could be useful for special observations requiring very high angular resolution of strong sources, for example, for the burst radiation from Jupiter. However, RadioAstron provides baselines almost as long.

1.4 Quantum Effect

The development of VLBI introduced a new facet into the apparent paradox in the quantum-mechanical description of interferometry (Burke 1969). The radio interferometer is the analog of Young's two-slit interference experiment. It is well known (Loudon 1973) that a single photon creates an interference pattern but that any attempt to determine which slit the photon entered will destroy the interference pattern; otherwise, the uncertainty principle would be violated. Consideration of VLBI suggests that it might be possible to determine at which antenna a particular photon arrived, since its signature is captured in the medium used for transmission to the correlator as well as in the fringe pattern generated during correlation. However, in the radio frequency range, the input stages of receivers used as the measurement devices consist of amplifiers or mixers that conserve the received phase in their outputs. This allows formation of the fringes in subsequent stages. The response of such devices must be consistent with the uncertainty principle, $\Delta E \Delta t \simeq h/2\pi$, where ΔE and Δt are the uncertainties in signal energy and measurement time. This principle can be written in terms of uncertainty in photon number, ΔN_p, and phase, $\Delta\phi$, as

$$\Delta N_p \, \Delta\phi \simeq 1 \, , \tag{1.15}$$

where $\Delta N_p = \Delta E/h\nu$ and $\Delta\phi = 2\pi\nu\Delta t$. To preserve phase, $\Delta\phi$ must be small, so ΔN_p must be correspondingly large, and there must be an uncertainty of at least one photon per unit bandwidth per unit time in the output of the receiving amplifier. Hence, the SNR is less than unity in the single-photon limit, and it is impossible to determine at which antenna a single photon entered. An alternative but equivalent statement is that the output of any receiving system must contain a noise component that is not less than an equivalent input power approximately equal to $h\nu$ per unit bandwidth.

The individual photons that constitute a radio signal arrive at antennas at random times but with an average rate that is proportional to the signal strength. For

phenomena of this type, the number of events that occur in a given time interval τ varies statistically in accordance with the Poisson distribution. For a signal power $P_{\rm sig}$, the average number of photons that arrive within time τ is $\overline{N_p} = P_{\rm sig}\tau/h\nu$. The rms deviation of the number arriving during a series of intervals τ is, for Poisson statistics, given by $\Delta N_p = \sqrt{\overline{N_p}}$. From Eq. (1.15), the resulting uncertainty in the signal phase is

$$\Delta\phi \simeq \frac{1}{\sqrt{\overline{N_p}}} = \sqrt{\frac{h\nu}{P_{\rm sig}\tau}} \,. \tag{1.16}$$

We can also express the uncertainty in the measurement of the signal phase in terms of the noise that is present in the receiving system. The minimum noise power, $P_{\rm noise}$, is approximately equal to the thermal noise from a matched resistive load at temperature $h\nu/k$, that is, $P_{\rm noise} = h\nu\Delta\nu$. The uncertainty in the phase, as measured with an averaging time τ, becomes

$$\Delta\phi = \sqrt{\frac{P_{\rm noise}}{P_{\rm sig}\tau\Delta\nu}} \,. \tag{1.17}$$

Note that $\Delta\phi$ is the accuracy with which the phase of the amplified signal received from one antenna can be measured: for example, in Doppler tracking of a spacecraft (Cannon 1990). This is not to be confused with the accuracy of measurement of the fringe phase of an interferometer. For a frequency $\nu = 1$ GHz, the effective noise temperature $h\nu/k$ is equal to 0.048 K. Thus, for frequencies up to some tens of gigahertz, the quantum effect noise makes only a small contribution to the receiver noise. At 900 GHz, which is generally considered to be about the high frequency limit for ground-based radio astronomy, $h\nu/k = 43$ K, and the contribution to the system noise is becoming important. In the optical region, $\nu \approx 500$ THz, $h\nu/k \approx 30,000$ K, and heterodyne systems are of limited practicality, as discussed in Sect. 17.6.2. However, in the optical region, it is possible to build "direct detection" devices that detect power without conserving phase, so $\Delta\phi$ in Eq. (1.17) effectively tends to infinity, and there is no constraint on the measurement accuracy of the number of photons. Thus, most optical interferometers form fringes directly from the light received and measure the resulting patterns of light intensity to determine the fringe parameters.

For further reading on the general subject of thermal and quantum noise, see, for example, Oliver (1965) and Kerr et al. (1997). Nityananda (1994) compares quantum issues in the radio and optical domains, and a discussion of basic concepts is given by Radhakrishnan (1999).

Appendix 1.1 Sensitivity of Radio Astronomical Receivers (the Radiometer Equation)

An idealized block diagram of the basic receiver configuration widely used in radio astronomy is shown in Fig. A1.1. We describe its function and analyze its performance in this appendix. The signal from an antenna is first passed through an amplifier. The amplifier is characterized by its power gain factor, G; receiver temperature; and the bandwidth, $\Delta\nu$. The gain factor is assumed to be constant. If the gain is sufficiently high, this amplifier sets the noise performance of the entire system, which we denote as T_S to include the contributions from atmosphere, ground pickup, and ohmic losses. We assume that the passband has a rectangular shape that is flat between a lower cutoff frequency, ν_0, and the upper cutoff frequency, $\nu_0 + \Delta\nu$. The signal then passes through a mixer, where it is multiplied by a sinusoidal local oscillator signal at frequency ν_0 and is converted to a baseband from 0 to $\Delta\nu$. In the next stage, the signal is converted to a digital data stream sampled at the Nyquist rate. According to the Nyquist sampling theorem, a bandlimited signal can be represented by samples taken at intervals of $1/2\Delta\nu$. We assume there is no quantization error in this sampling process. In this case, the original signal can be exactly reconstructed from the sampled sequence by convolution with a sinc function. The sampled signal has the same statistical properties as the corresponding analog signal. The next step is a square-law detector, which squares the amplitudes of the signal samples. This is followed by an averager, which simply averages N samples in a running mean fashion. A system with these features is known as a single-sideband superheterodyne receiver (Armstrong 1921) or, simply, a total-power radiometer. Early interferometer receivers were a variation on this basic design (see Fig. 1.6): Signals from two antennas were added after the mixing stage before entering the square-law detector, and there was no signal digitization.

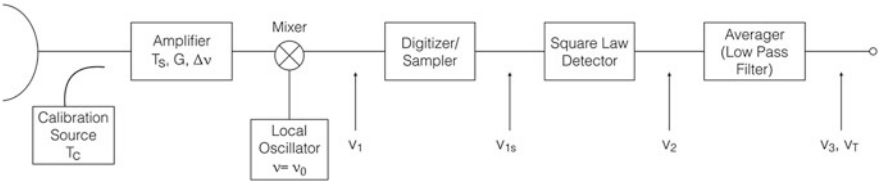

Fig. A1.1 A block diagram of an idealized radiometer used in most radio astronomical systems for measuring total power. The system temperature T_S includes the receiver temperature T_R plus all unwanted additive contributions (e.g., ohmic loses, atmospheric effects, ground pickup). In practice, at very low frequencies ($<$ 100 MHz), downconversion may be omitted, while at high frequencies (more than a few gigahertz), multiple stages of frequency downconversion are required. At very high frequencies ($>$ 100 GHz), where low noise amplifiers are not available, the first stage is usually the mixer. In this case, its losses and those of the amplifiers following it contribute to T_S.

The statistical performance of the idealized system in Fig. A1.1 can be readily evaluated. The power level at any point in the system can be characterized by a temperature T according to the Nyquist relation [e.g., Eq. (1.4)]

$$P = kT\Delta\nu\, G\,, \tag{A1.1}$$

where we have included the effect of power amplification by the gain factor G. The voltage v_1 is a combination of antenna input, characterized by T_A, and the additive system noise, T_S. We assume the cosmic input signal has a flat spectrum over the baseband frequency range. Hence, v_1 is a zero-mean Gaussian random process with a flat spectrum, i.e., a white noise spectrum. Such a process, described by $p(v)$, has only one parameter, the variance, σ^2. The odd moments of the probability distribution are zero, and the even moments are

$$\langle v^n\rangle = (1\cdot 3\cdot 5\cdot \ldots \cdot n)\,\sigma^n\,. \tag{A1.2}$$

The expectations of v_1 and v_1^2 (the power) are therefore

$$\langle v_1\rangle = 0\,, \tag{A1.3}$$

$$\langle v_1^2\rangle = k(T_S + T_A)\Delta\nu\, G\,. \tag{A1.4}$$

The statistics of the sampled signal, v_{1s}, and the analog signal v_1 are the same, i.e., $v_{1s} = v_1$, $v_{1s}^2 = v_1^2$, etc. The characteristics of v_2 are

$$\langle v_2\rangle = \langle v_1^2\rangle\,, \tag{A1.5}$$

$$\langle v_2^2\rangle = \langle v_1^4\rangle = 3\langle v_1^2\rangle^2\,, \tag{A1.6}$$

$$\sigma_2^2 = \langle v_2^2\rangle - \langle v_2\rangle^2 = 2\langle v_1^2\rangle^2\,. \tag{A1.7}$$

The averager averages $N = 2\Delta\nu\tau$ samples together, where τ is the integration time. Hence,

$$\langle v_3\rangle = \langle v_1^2\rangle = k(T_S + T_A)\Delta\nu\, G\,, \tag{A1.8}$$

$$\sigma_3^2 = \frac{\sigma_2^2}{N} = \frac{2[k(T_S + T_A)\Delta\nu\, G]^2}{2\Delta\nu\tau}\,. \tag{A1.9}$$

v_3 is converted from a power scale to a temperature scale by inserting a thermal noise signal of known temperature T_c in order to remove or calibrate the $k\Delta\nu\, G$ factor. Formally, the calibrated version of v_3 is

$$v_T = \frac{v_3}{\partial v_3/\partial T_A}\,, \tag{A1.10}$$

where $(\partial v_3/\partial T_A)^{-1}$ is the conversion factor from power to temperature written as a partial derivative. The mean and rms of the output in temperature units are therefore

$$\langle v_T \rangle = T_S + T_A \ , \tag{A1.11}$$

$$\sigma_T = \frac{T_S + T_A}{\sqrt{\Delta\nu\tau}} \ . \tag{A1.12}$$

It is important to note that the factor of two in the expression for σ_3^2 in Eq. (A1.8) cancels the factor of two in the number of samples averaged. The signal-to-noise ratio (SNR) is therefore

$$\mathcal{R}_{\rm sn} = \frac{T_A}{T_S + T_A}\sqrt{\Delta\nu\tau} \ . \tag{A1.13}$$

Equation (A1.13) shows that T_A contributes to the fluctuations, and in the limit $T_A \gg T_S$, longer integration does increase the SNR. For $T_A \ll T_S$, the usual case, Eq. (A1.13) becomes Eq. (1.8). Because of the fundamental limitation imposed by the Nyquist sampling theorem, no receiver system can perform better than specified by Eq. (A1.13). The performance of any other system can be written as

$$\sigma_T = C\,\frac{T_S + T_A}{\sqrt{\Delta\nu\tau}} \ , \tag{A1.14}$$

where C is a factor equal to, or greater than, one. The square-law detector could be replaced by another type of detector. For a linear detector, i.e., $v_2 = |v_1|$, a similar analysis to the one for the square-law detector yields $C = \sqrt{\pi - 2} = 1.07$ when $T_A \ll T_S$. In this calculation, it is necessary to linearize the output by calculation of $\partial v_3/\partial T_A$ in Eq. (A1.10). For a fourth-order detector, $v_2 = v_1^4$, $C = \sqrt{4/3} = 1.15$. More details can be found in Davenport and Root (1958).

G may not be a constant but can vary randomly due to electronic instabilities. In that case, a synchronous detector is added and receiver input is switched between the antenna and a reference signal. This system is known as a Dicke (1946) radiometer. (Note that the phase-switching interferometer [see Fig. 1.8] uses the synchronous detection principle.) The noise performance of a Dicke radiometer is worse by a factor of two, but the effects of gain fluctuations are mitigated. An alternative receiver that reduces the effects of gain fluctuations is called the correlation receiver, in which the signal from the antenna is divided in half and passed through separate amplifiers before being multiplied, where the multiplier replaces the square-law detector.

In older receivers, there was usually no digitization before the final averaging stage. The performance of a comparable analog system is identical to that described above. For analog analysis of radiometers, see Tiuri (1964) or Kraus (1986). A summary of the performance of various receiver types is given in Table A1.1.

Table A1.1 Sensitivity characteristics of various types of receivers

Receiver type	C[a]
Total power ($v_2 = v_1^2$)	1
Linear detector ($v_2 = \|v_1^2\|$)	1.07[b]
Fourth-order detector ($v_2 = v_1^4$)	1.15[b]
Dicke-switched receiver	2[b]
Correlation receiver	$\sqrt{2}$[b]

[a] C is defined in Eq. (A1.14).
[b] For $T_A \ll T_S$.

There are two major differences between radio and optical systems. Radio systems are characterized by Gaussian noise characteristics of both the signal and the additive receiver noise, whereas optical detectors are limited by Poisson statistics appropriate for counting photons and the SNR, $\mathcal{R}_{\text{sn}}$, is $1/\sqrt{N_p}$, where N_p is the number of photons. In terms of quantum mechanics, the Gaussian noise corresponds to photo bunching noise [see Radhakrishnan (1999)].

Further Reading

Textbooks on Radio Astronomy and Radio Interferometry

Burke, B.F., and Graham-Smith, F., *An Introduction to Radio Astronomy*, 3rd ed., Cambridge Univ. Press, Cambridge, UK (2014)

Christiansen, W.N., and Högbom, J.A., *Radiotelescopes*, Cambridge Univ. Press, Cambridge, UK (1969) (2nd ed., 1985)

Condon, J.J., and Ransom, S.M., *Essential Radio Astronomy*, Princeton Univ. Press, Princeton, NJ (2016)

Kraus, J.D., *Radio Astronomy*, 2nd ed., Cygnus-Quasar Books, Powell, OH, 1986. 1st ed., McGraw-Hill, New York (1966)

Lovell, B., and Clegg, J.A., *Radio Astronomy*, Chapman and Hall, London (1952)

Marr, J.M., Snell, R.L., and Kurtz, S.E., *Fundamentals of Radio Astronomy: Observational Methods*, CRC Press, Boca Raton, FL (2016)

Pawsey, J.L., and Bracewell, R.N., *Radio Astronomy*, Oxford Univ. Press, Oxford, UK (1955)
Shklovsky, I.S., *Cosmic Radio Waves*, translated by R. B. Rodman and C. M. Varsavsky, Harvard Univ. Press, Cambridge, MA (1960)
Wilson, T.L., Rohlfs, K., and Hüttemeister, S., *Tools of Radio Astronomy*, 6th ed., Springer-Verlag, Berlin (2013) (See also earlier editions, starting with K. Rohlfs, 1986.)
Wohlleben, R., Mattes, H., and Krichbaum, T., *Interferometry in Radioastronomy and Radar Techniques*, Kluwer, Dordrecht, the Netherlands (1991)

Historical Reviews

Kellermann, K.I., and Moran, J.M., The Development of High-Resolution Imaging in Radio Astronomy, *Ann. Rev. Astron. Astrophys.*, **39**, 457–509 (2001)
Sullivan, W.T., III, Ed., *The Early Years of Radio Astronomy*, Cambridge Univ. Press, Cambridge, UK (1984)
Sullivan, W.T., III, *Cosmic Noise: A History of Early Radio Astronomy*, Cambridge Univ. Press, Cambridge, UK (2009)
Townes, C.H., Michelson and Pease's Interferometric Stellar Diameters, *Astrophys. J.*, **525**, 148–149 (1999)

General Interest

Alder, B., Fernbach, S., Rotenberg, M., Eds., *Methods in Computational Physics*, Vol. 14, *Radio Astronomy*, Academic Press, New York (1975)
Berkner, L.V., Ed., *IRE Trans. Antennas Propag.*, Special Issue on Radio Astronomy, **AP-9**, No. 1 (1961)
Biraud, F., Ed., *Very Long Baseline Interferometry Techniques*, Cépaduès, Tou-louse, France (1983)
Bracewell, R.N., Ed., *Paris Symposium on Radio Astronomy*, IAU Symp. 9, Stanford Univ. Press, Stanford, CA (1959)
Bracewell, R.N., Radio Astronomy Techniques, in *Handbuch der Physik*, Vol. 54, S. Flugge, Ed., Springer-Verlag, Berlin (1962)
Cornwell, T.J., and Perley, R.A., Eds., *Radio Interferometry: Theory, Techniques, and Applications*, IAU Colloq. 131, Astron. Soc. Pacific Conf. Ser., **19** (1991)
Findlay, J.W., Ed., *Proc. IEEE*, Special Issue on Radio and Radar Astronomy, **61**, No. 9 (1973)
Frater, R.H., and Brooks, J.W., Eds., *J. Electric. Electron. Eng. Australia*, Special Issue on the Australia Telescope, **12**, No. 2 (1992)
Goldsmith, P.F., Ed., *Instrumentation and Techniques for Radio Astronomy*, IEEE Press, New York (1988)
Haddock, F.T., Ed., *Proc. IRE*, Special Issue on Radio Astronomy, **46**, No. 1 (1958)
Ishiguro, M., and Welch, W.J., Eds., *Astronomy with Millimeter and Submillimeter Wave Interferometry*, IAU Colloq. 140, Astron. Soc. Pacific Conf. Ser., **59** (1994)
Kraus, J.D., Ed., *IEEE Trans. Mil. Electron.*, Special Issue on Radio and Radar Astronomy, **MIL-8**, Nos. 3 and 4, 1964; also issued by *IEEE Trans. Antennas Propag.*, **AP-12**, No. 7 (1964)
Meeks, M.L., Ed., *Methods of Experimental Physics*, Vol. 12, Parts B, *Astrophysics: Radio Telescopes*, and C, *Astrophysics: Radio Observations*, Academic Press, New York (1976)
Pawsey, J.L., Ed., *Proc. IRE Aust.*, Special Issue on Radio Astronomy, **24**, No. 2 (1963)
Perley, R.A., Schwab, F.R., and Bridle, A.H., Eds., *Synthesis Imaging in Radio Astronomy*, Astron. Soc. Pacific Conf. Ser., **6** (1989)

Raimond, E., and Genee, R., Eds., *The Westerbork Observatory, Continuing Adventure in Radio Astronomy*, Kluwer, Dordrecht, the Netherlands (1996)
Taylor, G.B., Carilli, C.L., and Perley, R.A., Eds., *Synthesis Imaging in Radio Astronomy II*, Astron. Soc. Pacific Conf. Ser., **180** (1999)
Wild, J.P., Ed., *Proc. IREE Aust.*, Special Issue on the Culgoora Radioheliograph, **28**, No. 9 (1967)
Yen, J.L., Image Reconstruction in Synthesis Radio Telescope Arrays, in *Array Signal Processing*, Haykin, S., Ed., Prentice Hall, Englewood Cliffs, NJ (1985), pp. 293–350

References

Adgie, R.L., Gent, H., Slee, O.B., Frost, A.D., Palmer, H.P., and Rowson, B., New Limits to the Angular Sizes of Some Quasars, *Nature*, **208**, 275–276 (1965)
Appleton, E.V., Departure of Long-Wave Solar Radiation from Black-Body Intensity, *Nature*, **156**, 534–535 (1945)
Armstrong, E.H., A New System of Short Wave Amplification, *Proc. IRE*, **9**, 3–11 (1921)
Baade, W., and Minkowski, R., Identification of the Radio Sources in Cassiopeia, Cygnus A, and Puppis A, *Astrophys. J.*, **119**, 206–214 (1954a)
Baade, W., and Minkowski, R., On the Identification of Radio Sources, *Astrophys. J.*, **119**, 215–231 (1954b)
Baars, J.W.M., Genzel, R., Pauliny-Toth, I.I.K., and Witzel, A., The Absolute Spectrum of Cas A: An Accurate Flux Density Scale and a Set of Secondary Calibrators, *Astron. Astrophys*, **61**, 99–106 (1977)
Baars, J.W.M., van der Brugge, J.F., Casse, J.L., Hamaker, J.P., Sondaar, L.H., Visser, J.J., and Wellington, K.J., The Synthesis Radio Telescope at Westerbork, *Proc. IEEE*, **61**, 1258–1266 (1973)
Backer, D.C., and Sramek, R.A., Proper Motion of the Compact, Nonthermal Radio Source in the Galactic Center, Sagittarius A*, *Astrophys. J.*, **524**, 805–815 (1999)
Bare, C., Clark, B.G., Kellermann, K.I., Cohen, M.H., and Jauncey, D.L., Interferometer Experiment with Independent Local Oscillators, *Science*, **157**, 189–191 (1967)
Beevers, C.A., and Lipson, H., A Brief History of Fourier Methods in Crystal-Structure Determination, *Aust. J. Phys.*, **38**, 263–271 (1985)
Bennett, A.S., The Revised 3C Catalog of Radio Sources, *Mem. R. Astron. Soc.*, **68**, 163–172 (1962)
Blake, G.A., Sutton, E.C., Masson, C.R., and Phillips, T.G., Molecular Abundances in OMC-1: The Chemical Composition of Interstellar Molecular Clouds and the Influence of Massive Star Formation, *Astrophys. J.*, **315**, 621–645 (1987)
Blum, E.J., Le Réseau Nord-Sud à Multiples, *Ann. Astrophys.*, **24**, 359–366 (1961)
Blum, E.J., Boischot, A., and Ginat, M., Le Grand Interféromètre de Nançay, *Ann. Astrophys.*, **20**, 155–164 (1957)
Blythe, J.H., A New Type of Pencil Beam Aerial for Radio Astronomy, *Mon. Not. R. Astron. Soc.*, **117**, 644–651 (1957)
Boccardi, B., Krichbaum, T.P., Bach, U., Mertens, F., Ros, E., Alef, W., and Zensus, J.A., The Stratified Two-Sided Jet of Cygnus A, *Astron. Astrophys.*, **585**, A33 (9pp) (2016)
Bolton, J.G., and Slee, O.B., Galactic Radiation at Radio Frequencies. V. The Sea Interferometer, *Aust. J. Phys.*, **6**, 420–433 (1953)
Bolton, J.G., and Stanley, G.J., Variable Source of Radio Frequency Radiation in the Constellation of Cygnus, *Nature*, **161**, 312–313 (1948)
Born, M., and Wolf, E., *Principles of Optics*, 1st ed., Pergamon Press Ltd., London (1959) [many subsequent editions, e.g., 7th ed., Cambridge Univ. Press, Cambridge, UK, 1999]

Braccesi, A., Ceccarelli, M., Colla, G., Fanti, R., Ficarra, A., Gelato, G., Greuff, G., and Sinigaglia, G., The Italian Cross Radio Telescope. III. Operation of the Telescope, *Nuovo Cimento B*, **62**, 13–19 (1969)

Bracewell, R.N., and Swarup, G., The Stanford Microwave Spectroheliograph Antenna, a Microsteradian Pencil Beam Interferometer, *IRE Trans. Antennas Propag.*, **AP-9**, 22–30 (1961)

Broten, N.W., Early Days of Canadian Long-Baseline Interferometry: Reflections and Reminiscences, *J. Roy. Astron. Soc. Can.*, **82**, 233–241 (1988)

Broten, N.W., Legg, T.H., Locke, J.L., McLeish, C.W., Richards, R.S., Chisholm, R.M., Gush, H.P., Yen, J.L., and Galt, J.A., Observations of Quasars Using Interferometer Baselines Up to 3,074 km, *Nature*, **215**, 38 (1967)

Brown, G.W., Carr, T.D., and Block, W.F., Long Baseline Interferometry of S-Bursts from Jupiter, *Astrophys. Lett.*, **1**, 89–94 (1968)

Burke, B.F., Quantum Interference Paradox, *Nature*, **223**, 389–390 (1969)

Burke, B.F., Johnston, K.J., Efanov, V.A., Clark, B.G., Kogan, L.R., Kostenko, V.I., Lo, K.Y., Matveenko, L.I., Moiseev, I.G., Moran, J.M., and five coauthors, Observations of Maser Radio Source with an Angular Resolution of 0.″0002, *Sov. Astron.-AJ*, **16**, 379–382 (1972)

Cannon, A.J., and Pickering, E.C., The Henry Draper Catalogue, 21^{h}, 22^{h}, and 23^{h}, *Annals of the Astronomical Observatory of Harvard College*, **99** (1924)

Cannon, W.H., Quantum Mechanical Uncertainty Limitations on Deep Space Navigation by Doppler Tracking and Very Long Baseline Interferometry, *Radio Sci.*, **25**, 97–100 (1990)

Carilli, C.L., Bartel, N., and Diamond, P., Second Epoch VLBI Observations of the Nuclear Jet in Cygnus A: Subluminal Jet Proper Motion Measured, *Astron. J.*, **108**, 64–75 (1994). doi: 10.1086/117045

Christiansen, W.N., and Mullaly, R.F., Solar Observations at a Wavelength of 20 cm with a Cross-Grating Interferometer, *Proc. IRE Aust.*, **24**, 165–173 (1963)

Christiansen, W.N., and Warburton, J.A., The Distribution of Radio Brightness over the Solar Disk at a Wavelength of 21 cm. III. The Quiet Sun. Two-Dimensional Observations, *Aust. J. Phys.*, **8**, 474–486 (1955)

Clark, B.G., Radio Interferometers of Intermediate Type, *IEEE Trans. Antennas Propag.*, **AP-16**, 143–144 (1968)

Clark, B.G., Radhakrishnan, V., and Wilson, R.W., The Hydrogen Line in Absorption, *Astrophys. J.*, **135**, 151–174 (1962)

Clark, T.A., Corey, A.E., Davis, J.L., Elgered, G., Herring, T.A., Hinteregger, H.F., Knight, C.A., Levine, J.I., Lundqvist, G., Ma, C., and 11 coauthors, Precision Geodesy Using the Mark-III Very-Long-Baseline Interferometer System, *IEEE Trans. Geosci. Remote Sens.*, **GE-23**, 438–449 (1985)

Cohen, M.H., Cannon, W., Purcell, G.H., Shaffer, D.B., Broderick, J.J., Kellermann, K.I., and Jauncy, D.L., The Small-Scale Structure of Radio Galaxies and Quasi-Stellar Sources, at 3.8 Centimeters, *Astrophys. J.*, **170**, 202–217 (1971)

Cohen, M.H., Moffet, A.T., Romney, J.D., Schilizzi, R.T., Shaffer, D.B., Kellermann, K.I., Purcell, G.H., Grove, G., Swenson, G.W., Jr., Yen, J.L., and four coauthors, Observations with a VLB Array. I. Introduction and Procedures, *Astrophys. J.*, **201**, 249–255 (1975)

Condon, J.J., Confusion and Flux-Density Error Distributions, *Astrophys. J.*, **188**, 279–286 (1974)

Condon, J.J., Radio Emission from Normal Galaxies, *Ann. Rev. Astron. Astrophys.*, **30**, 575–611 (1992)

Condon, J.J., Cotton, W.D., Fomalont, E.B., Kellermann, K.I., Miller, N., Perley, R.A., Scott, D., Vernstrom, T., and Wall, J.V., Resolving the Radio Source Background: Deeper Understanding Through Confusion, *Astrophys. J.*, **758**:23 (14pp) (2012)

Condon, J.J., Cotton, W.D., Greisen, E.W., Yin, Q.F., Perley, R.A., Taylor, G.B., and Broderick, J.J., The NRAO VLA Sky Survey, *Astron. J.*, **115**, 1693–1716 (1998)

Covington, A.E., and Broten, N.W., An Interferometer for Radio Astronomy with a Single-Lobed Radiation Pattern, *Proc. IRE Trans. Antennas Propag.*, **AP-5**, 247–255 (1957)

Davenport, W.B., Jr. and Root, W.L., *An Introduction to the Theory of Random Signals and Noise*, McGraw-Hill, New York (1958)

de Bruijne, J.H.J., Rygl, K.L.J., and Antoja, T., GAIA Astrometric Science Performance: Post-Launch Predictions, *EAS Publications Ser.*, **67–68**, 23–29 (2014)

Dicke, R.H., The Measurement of Thermal Radiation at Microwave Frequencies, *Rev. Sci. Instrum.*, **17**, 268–275 (1946)

Dreyer, J.L.E., New General Catalog of Nebulae and Clusters of Stars, *Mem. R. Astron. Soc.*, **49**, Part 1 (1888) (reprinted *R. Astron. Soc. London*, 1962)

Edge, D.O., Shakeshaft, J.R., McAdam, W.B., Baldwin, J.E., and Archer, S., A Survey of Radio Sources at a Frequency of 159 Mc/s, *Mem. R. Astron. Soc.*, **68**, 37–60 (1959)

Elgaroy, O., Morris, D., and Rowson, B., A Radio Interferometer for Use with Very Long Baselines, *Mon. Not. R. Astron. Soc.*, **124**, 395–403 (1962)

Elitzur, M., *Astronomical Masers*, Kluwer, Dordrecht, the Netherlands (1992)

Fey, A.L., Gordon, D., Jacobs, C.S., Ma, C., Gamme, R.A., Arias, E.F., Bianco, G., Boboltz, D.A., Böckmann, S., Bolotin, S., and 31 coauthors, The Second Realization of the International Celestial Reference Frame by Very Long Baseline Interferometry, *Astrophys. J.*, **150**:58 (16pp) (2015)

Fomalont, E.B., The East–West Structure of Radio Sources at 1425 MHz, *Astrophys. J. Suppl.*, **15**, 203–274 (1968). doi: 10.1086/190166F

Genzel, R., Reid, M.J., Moran, J.M., and Downes, D., Proper Motions and Distances of H_2O Maser Sources. I. The Outflow in Orion-KL, *Astrophys. J.*, **244**, 884–902 (1981)

Gold, T., Radio Method for the Precise Measurement of the Rotation Period of the Earth, *Science*, **157**, 302–304 (1967)

Gower, J.F.R., Scott, P.F., and Wills, D., A Survey of Radio Sources in the Declination Ranges −07° to 20° and 40° to 80°, *Mem. R. Astron. Soc.*, **71**, 49–144 (1967)

Gray, M., *Maser Sources in Astrophysics*, Cambridge Univ. Press, Cambridge, UK (2012)

Guilloteau, S., The IRAM Interferometer on Plateau de Bure, in *Astronomy with Millimeter and Submillimeter Wave Interferometry*, Ishiguro, M., and Welch, W.J., Eds., Astron. Soc. Pacific Conf. Ser., **59**, 27–34 (1994)

Gurwell, M.A., Muhleman, D.O., Shah, K.P., Berge, G.L., Rudy, D.J., and Grossman, A.W., Observations of the CO Bulge on Venus and Implications for Mesospheric Winds, *Icarus*, **115**, 141–158 (1995)

Hagfors, T., Phillips, J.A., and Belcora, L., Radio Interferometry by Lunar Reflections, *Astrophys. J.*, **362**, 308–317 (1990)

Hanbury Brown, R., Measurement of Stellar Diameters, *Ann. Rev. Astron. Astrophys.*, **6**, 13–38 (1968)

Hanbury Brown, R., Palmer, H.P., and Thompson, A.R., A Rotating-Lobe Interferometer and Its Application to Radio Astronomy, *Philos. Mag.*, Ser. 7, **46**, 857–866 (1955)

Hanbury Brown, R., and Twiss, R.Q., A New Type of Interferometer for Use in Radio Astronomy, *Philos. Mag.*, Ser. 7, **45**, 663–682 (1954)

Hargrave, P.J., and Ryle, M., Observations of Cygnus A with the 5-km Radio Telescope, *Mon. Not. R. Astron. Soc.*, **166**, 305–327 (1974)

Harvey, P.M., Thronson, H.A., Jr., and Gatley, I., Far-Infrared Observations of Optical Emission-Line Stars: Evidence for Extensive Cool Dust Clouds, *Astrophys. J.*, **231**, 115–123 (1979)

Hazard, C., and Walsh, D., A Comparison of an Interferometer and Total-Power Survey of Discrete Sources of Radio Frequency Radiation, in *The Paris Symposium on Radio Astronomy*, Bracewell, R.N., Ed., Stanford Univ. Press, Stanford, CA (1959), pp. 477–486

Herbst, E., and van Dishoeck, E.F., Complex Organic Interstellar Moledules, *Ann. Rev. Astron. Astrophpys.*, **47**, 427–480 (2009)

Herring, T.A., Shapiro, I.I., Clark, T.A., Ma, C., Ryan, J.W., Schupler, B.R., Knight, C.A., Lundqvist, G., Shaffer, D.B., Vandenberg, N.R., and nine coauthors, Geodesy by Radio Interferometry: Evidence for Contemporary Plate Motion, *J. Geophys. Res.*, **91**, 8344–8347 (1986)

Herrnstein, J.R., Moran, J.M., Greenhill, L.J., Diamond, P.J., Inoue, M., Nakai, N., Miyoshi, M., Henkel, C., and Riess, A., A Geometric Distance to the Galaxy NGC4258 from Orbital Motions in a Nuclear Gas Disk, *Nature*, **400**, 539–841 (1999)

Herrnstein, J.R., Moran, J.M., Greenhill, L.J., and Trotter, A.S., The Geometry of and Mass Accretion Rate Through the Maser Accretion Disk in NGC4258, *Astrophys. J.*, **629**, 719–738 (2005). doi: 10.1086/431421

Hirabayashi, H., Hirosawa, H., Kobayashi, H., Murata, Y., Edwards, P.G., Fomalont, E.B., Fujisawa, K., Ichikawa, T., Kii, T., Lovell, J.E.J., and 43 coauthors, Overview and Initial Results of the Very Long Baseline Interferometry Space Observatory Programme, *Science*, **281**, 1825–1829 (1998)

Ho, P.T.P., Moran, J.M., and Lo, K.Y., The Submillimeter Array, *Astrophys. J. Lett.*, **616**, L1–L6 (2004)

Hogg, D.E., Macdonald, G.H., Conway, R.G., and Wade, C.M., Synthesis of Brightness Distribution in Radio Sources, *Astron. J.*, **74**, 1206–1213 (1969)

Hughes, M.P., Thompson, A.R., Colvin, R.S., An Absorption-Line Study of Galactic Neutral Hydrogen at 21 cm Wavelength, *Astrophys. J. Suppl.*, **23**, 232–367 (1971)

Humphreys, E.M.L., Reid, M.J., Moran, J.M., Greenhill, L.J., and Argon, A.L., Toward a New Geometric Distance to the Active Galaxy NGC 4258. III. Final Results and the Hubble Constant, *Astrophys. J.*, **775**:13 (10pp) (2013)

International Astronomical Union, *Trans. Int. Astron. Union*, Proc. of the 15th General Assembly Sydney 1974 and Extraordinary General Assembly Poland 1973, Contopoulos, G., and Jappel, A., Eds., **15B**, Reidel, Dordrecht, the Netherlands (1974), p. 142

International Astronomical Union, Specifications Concerning Designations for Astronomical Radiation Sources Outside the Solar System (2008). http://vizier.u-strasbg.fr/vizier/Dic/iau-spec.htx

IEEE, Standard Definitions of Terms for Radio Wave Propagation, Std. 211–1977, Institute of Electrical and Electronics Engineers Inc., New York (1977)

Jansky, K.G., Electrical Disturbances Apparently of Extraterrestrial Origin, *Proc. IRE*, **21**, 1387–1398 (1933)

Jennison, R.C., A Phase Sensitive Interferometer Technique for the Measurement of the Fourier Transforms of Spatial Brightness Distributions of Small Angular Extent, *Mon. Not. R. Astron. Soc.*, **118**, 276–284 (1958)

Jennison, R.C., High-Resolution Imaging Forty Years Ago, in *Very High Angular Resolution Imaging*, IAU Symp. 158, J. G. Robertson and W. J. Tango, Eds., Kluwer, Dordrecht, the Netherlands (1994), pp. 337–341

Jennison, R.C., and Das Gupta, M.K., Fine Structure in the Extra-terrestrial Radio Source Cygnus 1, *Nature*, **172**, 996–997 (1953)

Jennison, R.C., and Das Gupta, M.K., The Measurement of the Angular Diameter of Two Intense Radio Sources, Parts I and II, *Philos. Mag.*, Ser. 8, **1**, 55–75 (1956)

Jennison, R.C., and Latham, V., The Brightness Distribution Within the Radio Sources Cygnus A (19N4A) and Cassiopeia (23N5A), *Mon. Not. R. Astron. Soc.*, **119**, 174–183 (1959)

Jet Propulsion Laboratory, molecular spectroscopy site of JPL (2016). https://spec.jpl.nasa.gov

Kardashev, N.S., Khartov, V.V., Abramov, V.V., Avdeev, V.Yu., Alakoz, A.V., Aleksandrov, Yu.A., Ananthakrishnan, S., Andreyanov, V.V., Andrianov, A.S., Antonov, N.M., and 120 coauthors, "RadioAstron": A Telescope with a Size of 300,000 km: Main Parameters and First Observational Results, *Astron. Reports*, **57**, 153–194 (2013)

Kaula, W., Ed., *The Terrestrial Environment: Solid-Earth and Ocean Physics*, NASA Contractor Report 1579, NASA, Washington, DC (1970). http://ilrs.gsfc.nasa.gov/docs/williamstown_1968.pdf

Kellermann, K.I., The Discovery of Quasars, *Bull. Astr. Soc. India*, **41**, 1–17 (2013)

Kellermann, K.I., and Cohen, M.H., The Origin and Evolution of the N.R.A.O.–Cornell VLBI System, *J. Roy. Astron. Soc. Can.*, **82**, 248–265 (1988)

Kellermann, K.I., and Moran, J.M., The Development of High-Resolution Imaging in Radio Astronomy, *Ann. Rev. Astron. Astrophys.*, **39**, 457–509 (2001)

Kellermann, K.I., and Pauliny-Toth, I.I.K., The Spectra of Opaque Radio Sources, *Astrophys. J. Lett.*, **155**, L71–L78 (1969)

Kerr, A.R., Feldman, M.J., and Pan, S.-K., Receiver Noise Temperature, the Quantum Noise Limit, and the Role of Zero-Point Fluctuations, *Proc. 8th Int. Symp. Space Terahertz Technology*, 1997, pp. 101–111; also available as MMA Memo 161, National Radio Astronomy Observatory (1997)

Kesteven, M.J.L., and Bridle, A.H., Index of Extragalactic Radio-Source Catalogues, *Royal Astron. Soc. Canada J.*, **71**, 21–39 (1971)

Knowles, S.H., Waltman, W.B., Yen, J.L., Galt, J., Fort, D.N., Cannon, W.H., Davidson, D., Petrachenko, W., and Popelar, J., A Phase-Coherent Link via Synchronous Satellite Developed for Very Long Baseline Radio Interferometry, *Radio Sci.*, **17**, 1661–1670 (1982)

Kraus, J.D., *Radio Astronomy*, 2nd ed., Cygnus-Quasar Books, Powell, OH (1986)

Labrum, N.R., Harting, E., Krishnan, T., and Payten, W.J., A Compound Interferometer with a 1.5 Minute of Arc Fan Beam, *Proc. IRE Aust.*, **24**, 148–155 (1963)

Lequeux, J., Mesures Interférométriques à Haute Résolution du Diamètre et de la Structure des Principales Radiosources à 1420 MHz, *Annales d'Astrophysique*, **25**, 221–260 (1962)

Levy, G.S., Linfield, R.P., Edwards, C.D., Ulvestad, J.S., Jordan, J.F., Jr., Dinardo, S.J., Christensen, C.S., Preston, R.A., Skjerve, L.J., Stavert, L.R., and 22 coauthors, VLBI Using a Telescope in Earth Orbit. I. The Observations, *Astrophys. J.*, **336**, 1098–1104 (1989)

Linfield, R., VLBI Observations of Jets in Double Radio Galaxies, *Astrophys. J.*, **244**, 436–446 (1981)

Linfield, R.P., Levy, G.S., Edwards, C.D., Ulvestad, J.S., Ottenhoff, C.H., Hirabayashi, H., Morimoto, M., Inoue, M., Jauncey, D.L., Reynolds, J., and 18 coauthors, 15 GHz Space VLBI Observations Using an Antenna on a TDRSS Satellite, *Astrophys. J.*, **358**, 350–358 (1990)

Linfield, R.P., Levy, G.S., Ulvestad, J.S., Edwards, C.D., DiNardo, S.J., Stavert, L.R., Ottenhoff, C.H., Whitney, A.R., Cappallo, R.J., Rogers, A.E.E., and five coauthors, VLBI Using a Telescope in Earth Orbit. II. Brightness Temperatures Exceeding the Inverse Compton Limit, *Astrophys. J.*, **336**, 1105–1112 (1989)

Longair, M.S., *High Energy Astrophysics*, 2 vols., Cambridge Univ. Press, Cambridge, UK (1992)

Loudon, R., *The Quantum Theory of Light*, Oxford Univ. Press, London (1973), p. 229

Lovas, F.J., Recommended Rest Frequencies for Observed Interstellar Molecular Microwave Transitions—1991 Revision, *J. Phys. and Chem. Ref. Data*, **21**, 181–272 (1992)

Lovas, F.J., Snyder, L.E., and Johnson, D.R., Recommended Rest Frequencies for Observed Interstellar Molecular Transitions, *Astrophys. J. Suppl.*, **41**, 451–480 (1979)

Ma, C., Arias, E.F., Eubanks, T.M., Fey, A.L., Gontier, A.-M., Jacobs, C.S., Sovers, O.J., Archinal, B.A., and Charlot, P., The International Celestial Reference Frame as Realized by Very Long Baseline Interferometry, *Astron. J.*, **116**, 516–546 (1998)

Maltby, P., and Moffet, A.T., Brightness Distribution in Discrete Radio Sources. III. The Structure of the Sources, *Astrophys. J. Suppl.*, **7**, 141–163 (1962)

Matveenko, L.I., Kardashev, N.S., and Sholomitskii, G.B., Large Baseline Radio Interferometers, *Radiofizika*, **8**, 651–654 (1965); Engl. transl. in *Sov. Radiophys.*, **8**, 461–463 (1965)

McCready, L.L., Pawsey, J.L., and Payne-Scott, R., Solar Radiation at Radio Frequencies and Its Relation to Sunspots, *Proc. R. Soc. London A*, **190**, 357–375 (1947)

Menu, J., van Boekel, R., Henning, Th., Chandler, C.J., Linz, H., Benisty, M., Lacour, S., Min, M., Waelkens, C., Andrews, S.M., and 18 coauthors, On the Structure of the Transition Disk Around TW Hydrae, *Astron. Astrophys.*, **564**, A93 (22pp) (2014)

Messier, C., Catalogue des Nébuleuses et des Amas d'Étoiles [Catalogue of Nebulae and Star Clusters], *Connoissance des Temps* for 1784, 227–267, published in 1781. http://messier.seds.org/xtra/history/m-cat81.html

Michelson, A.A., On the Application of Interference Methods to Astronomical Measurements, *Philos. Mag.*, Ser. 5, **30**, 1–21 (1890)

Michelson, A.A., On the Application of Interference Methods to Astronomical Measurements, *Astrophys. J.*, **51**, 257–262 (1920)

Michelson, A.A., and Pease, F.G., Measurement of the Diameter of α Orionis with the Interferometer, *Astrophys. J.*, **53**, 249–259 (1921)

Mills, B.Y., The Positions of the Six Discrete Sources of Cosmic Radio Radiation, *Aust. J. Sci. Res.*, **A5**, 456–463 (1952)
Mills, B.Y., The Radio Brightness Distribution Over Four Discrete Sources of Cosmic Noise, *Aust. J. Phys.*, **6**, 452–470 (1953)
Mills, B.Y., Cross-Type Radio Telescopes, *Proc. IRE Aust.*, **24**, 132–140 (1963)
Mills, B.Y., Aitchison, R.E., Little, A.G., and McAdam, W.B., The Sydney University Cross-Type Radio Telescope, *Proc. IRE Aust.*, **24**, 156–165 (1963)
Mills, B.Y., and Little, A.G., A High Resolution Aerial System of a New Type, *Aust. J. Phys.*, **6**, 272–278 (1953)
Mills, B.Y., Little, A.G., Sheridan, K.V., and Slee, O.B., A High-Resolution Radio Telescope for Use at 3.5 m, *Proc. IRE*, **46**, 67–84 (1958)
Mills, B.Y., and Slee, O.B., A Preliminary Survey of Radio Sources in a Limited Region of the Sky at a Wavelength of 3.5 m, *Aust. J. Phys.*, **10**, 162–194 (1957)
Miyoshi, M., Moran, J., Herrnstein, J., Greenhill, L., Nakal, N., Diamond, P., and Inoue, M., Evidence for a Black Hole from High Rotation Velocities in a Sub-parsec Region of NGC4258, *Nature*, **373**, 127–129 (1995)
Moran, J.M., Thirty Years of VLBI: Early Days, Successes, and Future, in *Radio Emission from Galactic and Extragalactic Compact Sources*, J. A. Zensus, G. B. Taylor, and J. M. Wrobel, Eds., Astron. Soc. Pacific Conf. Ser., **144**, 1–10 (1998)
Moran, J.M., Crowther, P.P., Burke, B.F., Barrett, A.H., Rogers, A.E.E., Ball, J.A., Carter, J.C., and Bare, C.C., Spectral Line Interferometer with Independent Time Standards at Stations Separated by 845 Kilometers, *Science*, **157**, 676–677 (1967)
Morita, K.-I., The Nobeyama Millimeter Array, in *Astronomy with Millimeter and Submillimeter Wave Interferometry*, M. Ishiguro and W. J. Welch, Eds., Astron. Soc. Pacific Conf. Ser., **59**, 18–26 (1994)
Morris, D., Palmer, H.P., and Thompson, A.R., Five Radio Sources of Small Angular Diameter, *Observatory*, **77**, 103–106 (1957)
Napier, P.J., Bagri, D.S., Clark, B.G., Rogers, A.E.E., Romney, J.D., Thompson, A.R., and Walker, R.C., The Very Long Baseline Array, *Proc. IEEE*, **82**, 658–672 (1994)
Napier, P.J., Thompson, A.R., and Ekers, R.D., The Very Large Array: Design and Performance of a Modern Synthesis Radio Telescope, *Proc. IEEE*, **71**, 1295–1320 (1983)
NASA/IPAC Extragalactic Database, Best Practices for Data Publication to Facilitate Integration into NED: A Reference Guide for Authors, version 1.2, Sept. 25 (2013)
Nityananda, R., Comparing Optical and Radio Quantum Issues, in *Very High Resolution Imaging*, IAU Symp. 158, Robertson, J.G., and Tango, W.J., Eds., Kluwer, Dordrecht, the Netherlands (1994), pp. 11–18
Nyquist, H., Thermal Agitation of Electric Charge in Conductors, *Phys. Rev.*, **32**, 110–113 (1928)
O'Brien, P.A., The Distribution of Radiation Across the Solar Disk at Metre Wavelengths, *Mon. Not. R. Astron. Soc.*, **113**, 597–612 (1953)
Oliver, B.M., Thermal and Quantum Noise, *Proc. IEEE*, **53**, 436–454 (1965)
Pawsey, J.L., Sydney Investigations and Very Distant Radio Sources, *Publ. Astron. Soc. Pacific*, **70**, 133–140 (1958)
Pearson, T.J., Unwin, S.C., Cohen, M.H., Linfield, R.P., Readhead, A.C.S., Seielstad, G.A., Simon, R.S., and Walker, R.C., Superluminal Expansion of Quasar 3C273, *Nature*, **290**, 365–368 (1981)
Pease, F.G., Interferometer Methods in Astronomy, *Ergeb. Exakten Naturwiss.*, **10**, 84–96 (1931)
Perley, R.A., Dreher, J.W., and Cowan, J.J., The Jet and Filaments in Cygnus A, *Astrophys. J. Lett.*, **285**, L35–L38 (1984). doi: 10.1086/184360
Perley, R., Napier, P., Jackson, J., Butler, B., Carlson, B., Fort, D., Dewdney, P., Clark, B., Hayward, R., Durand, S., Revnell, M., and McKinnon, M., The Expanded Very Large Array, *Proc. IEEE*, **97**, 1448–1462 (2009)
Perryman, M.A.C., Lindegren, L., Kovalevsky, J., Høg, E., Bastian, U., Bernacca, P.L., Crézé, M., Donati, F., Grenon, M., Grewing, M., and ten coauthors, The Hipparcos Catalogue, *Astron. Astrophys.*, **323**, L49–L52 (1997)

Picken, J.S., and Swarup, G., The Stanford Compound-Grating Interferometer, *Astron. J.*, **69**, 353–356 (1964)

Radhakrishnan, V., Noise and Interferometry, in *Synthesis Imaging in Radio Astronomy II*, Taylor, G.B., Carilli, C.L., and Perley, R.A., Eds., Astron. Soc. Pacific Conf. Ser., **180**, 671–688 (1999)

Read, R.B., Two-Element Interferometer for Accurate Position Determinations at 960 Mc, *IRE Trans. Antennas Propag.*, **AP-9**, 31–35 (1961)

Reber, G., Cosmic Static, *Astrophys. J.*, **91**, 621–624 (1940)

Reid, M.J., and Brunthaler, A., The Proper Motion of Sagittarius A*. II. The Mass of Sagittarius A*, *Astrophys. J.*, **616**, 872–884 (2004)

Reid, M.J., Haschick, A.D., Burke, B.F., Moran, J.M., Johnston, K.J., and Swenson, G.W., Jr., The Structure of Interstellar Hydroxyl Masers: VLBI Synthesis Observations of W3(OH), *Astrophys. J.*, **239**, 89–111 (1980)

Reid, M.J., and Honma, M., Microarcsecond Radio Astrometry, *Ann. Rev. Astron. Astrophys.*, **52**, 339–372 (2014)

Reid, M.J., and Moran, J.M., Astronomical Masers, in *Galactic and Extragalactic Radio Astronomy*, 2nd ed., Verschuur, G.L., and Kellermann, K.I., Eds., Springer-Verlag, Berlin (1988), pp. 255–294

Roger, R.S., Costain, C.H., Lacey, J.D., Landaker, T.L., and Bowers, F.K., A Supersynthesis Radio Telescope for Neutral Hydrogen Spectroscopy at the Dominion Radio Astrophysical Observatory, *Proc. IEEE*, **61**, 1270–1276 (1973)

Rogers, A.E.E., Hinteregger, H.F., Whitney, A.R., Counselman, C.C., Shapiro, I.I., Wittels, J.J., Klemperer, W.K., Warnock, W.W., Clark, T.A., Hutton, L.K., and four coauthors, The Structure of Radio Sources 3C273B and 3C84 Deduced from the "Closure" Phases and Visibility Amplitudes Observed with Three-Element Interferometers, *Astrophys. J.*, **193**, 293–301 (1974)

Rowson, B., High Resolution Observations with a Tracking Radio Interferometer, *Mon. Not. R. Astron. Soc.*, **125**, 177–188 (1963)

Rybicki, G.B., and Lightman, A.P., *Radiative Processes in Astrophysics*, Wiley-Interscience, New York (1979) (reprinted 1985)

Ryle, M., A New Radio Interferometer and Its Application to the Observation of Weak Radio Stars, *Proc. R. Soc. London A*, **211**, 351–375 (1952)

Ryle, M., The New Cambridge Radio Telescope, *Nature*, **194**, 517–518 (1962)

Ryle, M., The 5-km Radio Telescope at Cambridge, *Nature*, **239**, 435–438 (1972)

Ryle, M., Radio Telescopes of Large Resolving Power, *Science*, **188**, 1071–1079 (1975)

Ryle, M., Elsmore, B., and Neville, A.C., High Resolution Observations of Radio Sources in Cygnus and Cassiopeia, *Nature*, **205**, 1259–1262 (1965)

Ryle, M., and Hewish, A., The Cambridge Radio Telescope, *Mem. R. Astron. Soc.*, **67**, 97–105 (1955)

Ryle, M., and Hewish, A., The Synthesis of Large Radio Telescopes, *Mon. Not. R. Astron. Soc.*, **120**, 220–230 (1960)

Ryle, M., Hewish, A., and Shakeshaft, J.R., The Synthesis of Large Radio Telescopes by the Use of Radio Interferometers, *IRE Trans. Antennas Propag.*, **7**, S120–S124 (1959)

Ryle, M., and Neville, A.C., A Radio Survey of the North Polar Region with a 4.5 Minute of Arc Pencil-Beam System, *Mon. Not. R. Astron. Soc.*, **125**, 39–56 (1962)

Ryle, M., and Smith, F.G., A New Intense Source of Radio Frequency Radiation in the Constellation of Cassiopeia, *Nature*, **162**, 462–463 (1948)

Ryle, M., Smith, F.G., and Elsmore, B., A Preliminary Survey of the Radio Stars in the Northern Hemisphere, *Mon. Not. R. Astron. Soc.*, **110**, 508–523 (1950)

Ryle, M., and Vonberg, D.D., Solar Radiation at 175 Mc/s, *Nature*, **158**, 339–340 (1946)

Scheuer, P.A.G., A Statistical Method for Analysing Observations of Faint Radio Stars, *Proc. Cambridge Phil. Soc.*, **53**, 764–773 (1957)

Schilke, P., Groesbeck, T., Blake, G.A., and Phillips, T.G., A Line Survey of Orion KL from 325 to 360 GHz, *Astrophys. J. uppl.*, **108**, 301–337 (1997)

Scoville, N., Carlstrom, J., Padin, S., Sargent, A., Scott, S., and Woody, D., The Owens Valley Millimeter Array, in *Astronomy with Millimeter and Submillimeter Wave Interferometry*, M. Ishiguro and W. J. Welch, Eds., Astron. Soc. Pacific Conf. Ser., **59**, 10–17 (1994)

Shakeshaft, J.R., Ryle, M., Baldwin, J.E., Elsmore, B., and Thomson, J.H., A Survey of Radio Sources Between Declinations -38° and +83°, *Mem. R. Astron. Soc.*, **67**, 106–154 (1955)

Smith, F.G., An Accurate Determination of the Positions of Four Radio Stars, *Nature*, **168**, 555 (1951)

Smith, F.G., The Determination of the Position of a Radio Star, *Mon. Not. R. Astron. Soc.*, **112**, 497–513 (1952a)

Smith, F.G., The Measurement of the Angular Diameter of Radio Stars, *Proc. Phys. Soc. B.*, **65**, 971–980 (1952b)

Smith, F.G., Apparent Angular Sizes of Discrete Radio Sources–Observations at Cambridge, *Nature*, **170**, 1065 (1952c)

Smoot, G.F., Bennett, C.L., Kogut, A., Wright, E.L., Aymon, J., Boggess, N.W., Cheng, E.S., de Amici, G., Gulkis, S., Hauser, M.G., and 18 coauthors, Structure in the COBE Differential Microwave Radiometer First-Year Maps, *Astrophys. J. Lett.*, **396**, L1–L5 (1992)

Smoot, G., Bennett, C., Weber, R., Maruschak, J., Ratliff, R., Janssen, M., Chitwood, J., Hilliard, L., Lecha, M., Mills, R., and 18 coauthors, COBE Differential Microwave Radiometers: Instrument Design and Implementation, *Astrophys. J.*, **360**, 685–695 (1990)

Southworth, G.C., Microwave Radiation from the Sun, *J. Franklin Inst.*, **239**, 285–297 (1945)

Splatalogue, database for astronomical spectroscopy (2016). http://www.cv.nrao.edu/php/splat

Swarup, G., Ananthakrishnan, S., Kapahi, V.K., Rao, A.P., Subrahmanya, C.R., and Kulkarni, V.K., The Giant Metrewave Radio Telescope, *Current Sci.* (Current Science Association and Indian Academy of Sciences), **60**, 95–105 (1991)

Thomasson, P., MERLIN, *Quart. J. R. Astron. Soc.*, **27**, 413–431 (1986)

Thompson, A.R., The Planetary Nebulae as Radio Sources, in *Vistas in Astronomy*, Vol. 16, A. Beer, Ed., Pergamon Press, Oxford, UK (1974), pp. 309–328

Thompson, A.R., Clark, B.G., Wade, C.M., and Napier, P.J., The Very Large Array, *Astrophys. J. Suppl.*, **44**, 151–167 (1980)

Thompson, A.R., and Krishnan, T., Observations of the Six Most Intense Radio Sources with a 1.0′ Fan Beam, *Astrophys. J.*, **141**, 19–33 (1965)

Tiuri, M.E., Radio Astronomy Receivers, *IEEE Trans. Antennas Propag.*, **AP-12**, 930–938 (1964)

University of Cologne, Physics Institute, Molecules in Space (2016). http://www.astro.uni-koeln.de/cdms/molecule

Vitkevich, V.V., and Kalachev, P.D., Design Principles of the FIAN Cross-Type Wide Range Telescope, in *Radio Telescopes*, Proc. P. N. Lebedev Phys. Inst. (Acad. Sci. USSR), Skobel'tsyn, D.V., Ed., Vol. 28, translated by Consultants Bureau, New York (1966)

Welch, W.J., The Berkeley–Illinois–Maryland Association Millimeter Array, in *Astronomy with Millimeter and Submillimeter Wave Interferometry*, Ishiguro, M., and Welch, W.J., Eds., Astron. Soc. Pacific Conf. Ser., **59**, 1–9 (1994)

Westerhout, G., A Survey of the Continuous Radiation from the Galactic System at a Frequency of 1390 Mc/s, *Bull. Astron. Inst. Netherlands*, **14**, 215–260 (1958)

Whitney, A.R., Lonsdale, C.J., and Fish, V.L., Insights into the Universe: Astronomy with Haystack's Radio Telescope, *Lincoln Lab. J.*, **21**, 8–27 (2014)

Whitney, A.R., Rogers, A.E.E., Hinteregger, H.F., Knight, C.A., Levine, J.I., Lippincott, S., Clark, T.A., Shapiro, I.I., and Robertson, D.S., A Very Long Baseline Interferometer System for Geodetic Applications, *Radio Sci.*, **11**, 421–432 (1976)

Whitney, A.R., Shapiro, I.I., Rogers, A.E.E., Robertson, D.S., Knight, C.A., Clark, T.A., Goldstein, R.M., Marandino, G.E., and Vandenberg, N.R., Quasars Revisited: Rapid Time Variations Observed via Very Long Baseline Interferometry, *Science*, **173**, 225–230 (1971)

Wootten, A., and Thompson, A.R., The Atacama Large Millimeter/Submillimeter Array, *Proc. IEEE*, **97**, 1463–1471 (2009)

Yen, J.L., Kellermann, K.I., Rayher, B., Broten, N.W., Fort, D.N., Knowles, S.H., Waltman, W.B., and Swenson, G.W., Jr., Real-Time, Very Long Baseline Interferometry Based on the Use of a Communications Satellite, *Science*, **198**, 289–291 (1977)